

# Impact-Generated Dust Clouds Surrounding the Galilean Moons

Harald Krüger<sup>1</sup>, Alexander V. Krivov<sup>2,3</sup>, Miodrag Sremčević<sup>2</sup>,  
and Eberhard Grün<sup>1,4</sup>

<sup>1</sup> Max-Planck-Institut für Kernphysik,  
Postfach 103980, 69029 Heidelberg, Germany  
E-Mail: Harald.Krueger@mpi-hd.mpg.de

<sup>2</sup> Nonlinear Dynamics Group, Institute of Physics, University of Potsdam,  
P.O. Box 601553, 14415 Potsdam, Germany  
E-mail: krivov@agnld.uni-potsdam.de

<sup>3</sup> On leave from: Astronomical Institute, St. Petersburg University,  
Stary Peterhof, 198504 St. Petersburg, Russia  
E-mail: krivov@astro.spbu.ru

<sup>4</sup> Hawaii Institute of Geophysics and Planetology, University of Hawaii,  
1680 East West Road, Honolulu, HI 96822, USA

Manuscript pages: 46  
Figures: 16  
Tables: 5

*Icarus*, in press

October 30, 2018

*Proposed Running Head:*

DUST CLOUDS OF THE GALILEAN MOONS

*Corresponding author:*

Harald Krüger  
Max-Planck-Institut für Kernphysik  
Postfach 103980  
69029 Heidelberg, Germany  
E-mail: Harald.Krueger@mpi-hd.mpg.de

## Abstract

Tenuous dust clouds of Jupiter’s Galilean moons Io, Europa, Ganymede and Callisto have been detected with the in-situ dust detector on board the Galileo spacecraft. The majority of the dust particles have been sensed at altitudes below five radii of these lunar-sized satellites. We identify the particles in the dust clouds surrounding the moons by their impact direction, impact velocity, and mass distribution. Average particle sizes are between 0.5 and  $1\ \mu\text{m}$ , just above the detector threshold, indicating a size distribution with decreasing numbers towards bigger particles. Our results imply that the particles have been kicked up by hypervelocity impacts of micrometeoroids onto the satellites’ surfaces. The measured radial dust density profiles are consistent with predictions by dynamical modeling for satellite ejecta produced by interplanetary impactors (Krivov et al., *Planet. Sp. Sci.*, 2003, 51, 251–269), assuming yield, mass and velocity distributions of the ejecta from laboratory measurements. A comparison of all four Galilean moons (data for Ganymede published earlier; Krüger et al., *Planet. Sp. Sci.*, 2000, 48, 1457–1471) shows that the dust clouds of the three outer Galilean moons have very similar properties and are in good agreement with the model predictions for solid ice-silicate surfaces. The dust density in the vicinity of Io, however, is more than an order of magnitude lower than expected from theory. This may be due to a softer, fluffier surface of Io (volcanic deposits) as compared to the other moons. The log-log slope of the dust number density in the clouds vs. distance from the satellite center ranges between  $-1.6$  and  $-2.8$ . Appreciable variations of number densities obtained from individual flybys with varying geometry, especially at Callisto, are found. These might be indicative of leading-trailing asymmetries of the clouds due to the motion of the moons with respect to the field of impactors.

### Keywords:

dust  
satellites of Jupiter  
planetary rings

# 1 Introduction

All celestial bodies without atmospheres are permanently exposed to bombardment by hypervelocity micrometeoroids which knock-off secondary ejecta dust particles from the surfaces of these bodies. Impact ejection of dust particles has been suggested as the main process for maintaining dusty planetary rings like the Jovian rings (Morfill et al., 1980; Horányi and Cravens, 1996; Ockert-Bell et al., 1999; Burns et al., 1999), Saturn's E ring (Horányi et al., 1992; Hamilton, D. P. and Burns, J. A., 1994) as well as putative dust belts of Mars (Soter, 1971; Krivov and Hamilton, 1997; Krivov and Jurewicz, 1999) and Pluto (Thiessenhusen et al., 2002). With the in-situ dust detector on board the Galileo spacecraft (Grün et al., 1992) a dust cloud formed by impact ejecta particles was for the first time detected surrounding Jupiter's moon Ganymede (Krüger et al., 1999d, 2000). The dust cloud was by far too tenuous to be detectable with remote sensing techniques. Particles belonging to the Ganymede dust cloud were identified by their impact direction and impact speed and their sizes were mostly below  $1\ \mu\text{m}$ . The spatial distribution of the grains as well as their size distribution were in agreement with model predictions based on the impact ejection mechanism.

The Galileo dust measurements can be treated as a natural impact experiment leading to the detection of the ejecta of hypervelocity impacts in space. They can give more insight into the process of hypervelocity dust ejection, for which the laboratory experiments on Earth still do not yield a comprehensive picture. The measurements of the dust cloud at Ganymede stimulated the development of analytical models for impact-generated circumsatellite dust clouds not only for the Galilean moons but also for the Saturnian satellites (Krivov et al., 2003; Sremčević et al., 2003). This is especially important for the dust measurements to be collected at Saturn with the dust instrument (Srama et al., 2002) onboard the Cassini spacecraft beginning in 2004.

Since December 1995 Galileo has been on a bound orbit about Jupiter. The spacecraft had a total of 32 targeted close flybys at all four Galilean moons: 7 encounters with Io, 11 with Europa, 6 with Ganymede and 8 with Callisto. During many of the encounters between 1995 and early 1999, the impact rate of dust grains showed a sharp peak within about half an hour centered at closest approach to the moon (Grün et al., 1996, 1997, 1998; Krüger et al., 1999a). These peaks indicated the existence of dust concentrations not only at Ganymede but also in the close vicinities of Io, Europa and Callisto. During the flybys at the Galilean moons after mid-1999, the spacecraft orientation prevented the detection of dust particles close to the satellites. In November 2002, Galileo had the only opportunity to in-situ measure dust in the close vicinity of a fifth Jovian moon: Amalthea (Krüger and Grün, 2002).

In addition to dust clouds surrounding the Galilean moons, at least three other populations of dust were detected by Galileo in the Jovian system (Grün et al., 1998). Streams of 10-nanometer dust particles were detected throughout the Jovian magnetosphere and were recognizable even in interplanetary space out to 2 AU from Jupiter (Grün et al., 1993; Grün et al., 1994). These dust grains originate from Io (Horányi et al., 1993a,b; Graps et al., 2000; Krüger et al., 2003a), their ultimate source probably being

the most powerful of Io’s volcanic plumes. Bigger, micrometer-sized particles form a tenuous dust ring between the Galilean moons and further away from Jupiter. Many of these particles orbit Jupiter on prograde orbits whereas a population on retrograde orbits exists as well (Colwell et al., 1998b; Thiessenhusen et al., 2000; Krivov et al., 2002a,b). An overview of the Galileo dust measurements at Jupiter including the dust instrument itself can be found in Krüger et al. (2003b).

A detailed analysis of the dust grains detected at Galileo’s four Ganymede flybys in 1996 and 1997 has been published earlier (Krüger et al., 1999d, 2000), showing that this Jovian moon is surrounded by a dust cloud formed by impact ejecta. Here, we analyze the dust impacts detected close to Io, Europa and Callisto, and compare our results with the measurements at Ganymede. Relevant physical properties of these moons are summarized in Table I. In Section 2 we give a brief overview of the most important aspects of the Galileo dust instrument, the Galileo spacecraft and the procedure to identify impacts of ejecta cloud particles in the Galileo dust data set. In Section 3 we analyze the dust detections at Io, Europa and Callisto. In Section 4 we compare the properties of the dust clouds of all four Galilean moons and check them against modeling. Section 5 lists our conclusions.

**Insert Table I**

## 2 Dust impact detection

### 2.1 Galileo dust instrument

The Galileo in-situ dust measurements at Ganymede provided the first in-situ detection of an impact-generated dust cloud in space (Krüger et al., 1999d). Processing of these measurements has been described in detail by Krüger et al. (2000). Here we apply the same analysis techniques to the dust measurements obtained in the close vicinities of Europa, Callisto and Io. Descriptions of the dust instrument, Galileo spacecraft, data transmission etc. have been published in previous papers. In what follows we recall only the most important aspects and give references to earlier publications where necessary.

Galileo is a dual-spinning spacecraft, with an antenna that points antiparallel to the positive spacecraft spin axis. During most of Galileo’s orbital mission about Jupiter, the antenna pointed towards Earth. The Galileo Dust Detector System (DDS), like its twin on-board Ulysses, is a multi-coincidence impact ionization detector (Grün et al., 1992) which measures submicrometer- and micrometer-sized dust impacts onto the detector target. The dust instrument is mounted on the spinning section of Galileo and its sensor axis is offset by an angle of  $60^\circ$  from the positive spin axis (Fig. 1). Thus, during one spin revolution of the spacecraft, the detector scans the entire anti-Earth hemisphere, whereas particles approaching from the Earth-ward direction remain undetectable.

For each dust grain hitting the detector target, three independent measurements of the impact-created plasma cloud are used to derive the impact speed  $v$  and the mass  $m$  of the particle. The charge  $Q_1$

released upon impact onto the target is described by the relation (Göller and Grün, 1989; Grün et al., 1995)

$$Q_1 \propto m \cdot v^{3.5}. \quad (1)$$

The calibrated speed range of the dust instrument is 2 to 70 km s<sup>-1</sup>. The coincidence times of the three charge signals together with the charges themselves are used to classify each impact into one of four categories. Class 3 impacts have three charge signals, two are required for class 2 and class 1 events, and only one for class 0 (Baguhl, 1993; Grün et al., 1995; Krüger et al., 1999b). Class 3 signals, our highest class, are real dust impacts and class 0 events are noise. Class 1 and class 2 events are true dust impacts in interplanetary space (Baguhl et al., 1993; Krüger et al., 1999b). However, in the Jovian system, within about 15R<sub>J</sub> distance from Jupiter, energetic particles from the Jovian plasma environment cause an enhanced noise rate in class 2 and the lower quality classes. By analysing the properties of the Io stream particles and comparing them with the noise events, the noise could be eliminated from the class 2 data (Krüger et al., 1999c). All class 0 and class 1 events detected in the Jovian environment are usually classified as noise.

Our noise identification scheme (Krüger et al., 1999c), however, was derived for the Jovian dust stream particles and, hence, its applicability to other populations of dust had to be verified. Since Europa orbits Jupiter within the region where the high noise rates occurred, a slightly modified scheme has been developed for the ejecta grains detected in the close vicinity of Europa (see Krüger et al., 2001, their Table 4). It will be applied in this paper to remove noise events from the data sets obtained at the flybys at Europa and Io. For the Callisto data, no noise removal is necessary because Callisto orbits Jupiter outside the region where the high noise rates occurred. Noise removal was also not necessary in the earlier analysis of the Ganymede data (Krüger et al., 2000). It has to be noted that the noise removal technique uses statistical arguments and is applicable to large data sets only. Individual dust impacts may be erroneously classified as noise and vice versa.

Galileo has a very low data transmission capability because its high-gain antenna did not open completely. For the dust measurements this means that the full set of parameters measured during a dust particle impact (spacecraft rotation angle, impact charges, charge rise times, etc.) could only be transmitted to Earth for a limited number of impact events. During the close satellite flybys at the Galilean moons these limits were between one event per minute (record mode) and one event per 21 minutes (real time science mode) (Krüger et al., 2001). When event rates (*i.e.* dust impacts plus noise) exceeded these numbers, the full set of parameters was transmitted to Earth for only a fraction of all detected events. All events, however, were always counted with one of 24 accumulators (Grün et al., 1995). This way, the data can be corrected for incomplete data transmission so that reliable impact rates can be determined for all satellite flybys (Krüger et al., 2000).

Since its injection into an orbit about Jupiter, the Galileo spacecraft has been exposed to the harsh radiation environment of the Jovian magnetosphere with energetic particles of up to several MeV energies. The Galileo Jupiter mission was extended three times so that the spacecraft was exposed to a total radiation dosage five times higher than it was originally designed for. Especially high radiation

dosages were acquired during orbit insertion in December 1995 and during several perijove passages after mid-1999 when Galileo’s perijove distance from Jupiter was about  $6 R_J$ . It was anticipated that these high radiation levels would cause severe damages to the spacecraft electronics and the scientific instruments. Although degradation of the dust instrument was recognised in the dust data, no failure has occurred so far. The degradation effects include – among others – a drop of the channeltron amplification, shifts of the measured instrument current, charge rise times and amplitudes which reduced the sensitivity for dust impacts and noise events (Krüger et al., in prep.). The most important effect for our analysis here is shifts in the speed and mass calibration of the dust impacts.

## 2.2 Impact direction

The analysis of the dust measurements obtained at Ganymede showed that the impact direction of the particles could be used as one important parameter to identify ejecta particles belonging to a dust cloud surrounding this moon (Krüger et al., 2000): in particular, the impact direction of the grains could be used to separate cloud particles from Jovian dust stream particles (Grün et al., 1998). As rotation angle,  $\Theta$ , we define the viewing direction of the dust sensor at the time of particle impact. During one spin revolution of the spacecraft, the rotation angle scans through  $360^\circ$ . Rotation angles for the Galileo dust instrument, however, are reported opposite to that of the actual spacecraft rotation direction. This is done to easily compare Galileo results with the dust detector data taken on the Ulysses spacecraft, which, unlike Galileo, has the opposite spin direction. Zero degrees of rotation angle is taken when the dust sensor points close to the ecliptic north direction. At rotation angles of  $90^\circ$  and  $270^\circ$  the sensor axis lies nearly in the ecliptic plane (which is close to Jupiter’s equatorial plane).

The dust instrument itself has a  $140^\circ$  wide field of view (FOV). Dust particles which arrive within  $10^\circ$  of the positive spin axis can be sensed at all rotation angles, while those that arrive at angles from  $10^\circ$  to  $130^\circ$  from the positive spin axis can only be sensed over a limited range of rotation angles. A sketch of the detection geometry at close satellite flybys is shown in Fig. 1.

## 2.3 Impact velocity

Calibrated impact velocities are derived from the rise times of the impact charge signals by an empirically derived algorithm (Grün et al., 1995). The analysis of the dust impacts detected close to Ganymede showed that their average impact velocity onto the detector target was close to the encounter velocity of Galileo with this moon ( $8 \text{ km s}^{-1}$ ) (Krüger et al., 2000). It implied that the particles truly originated from Ganymede and that they belonged to a steady-state dust cloud surrounding this satellite. This good agreement of the measured mean impact velocity with the expected velocity also showed that the calibration of the dust instrument is reliable in this velocity range.

Two statistical subsets of particles could be separated: nearly all of the Ganymede particles had

calibrated velocities below  $10 \text{ km s}^{-1}$ , whereas most of the stream particles had higher velocities. The calibrated impact velocity has been used as a parameter to separate both populations of dust at Galileo’s G8 Ganymede flyby when the Jovian stream particles approached the dust detector from the direction towards Ganymede and particles belonging to Ganymede’s steady-state dust cloud could not be identified by their impact direction alone. The true impact velocities of stream particles exceeded  $200 \text{ km s}^{-1}$  (Zook et al., 1996) and were much faster than the velocity range of the dust instrument calibrated in the laboratory ( $70 \text{ km s}^{-1}$ ). Thus, the velocities for the stream particles derived from the instrument calibration significantly underestimate the true particle velocities.

### 3 Data analysis

#### 3.1 Europa

##### 3.1.1 Impact direction

The antenna of Galileo usually pointed towards Earth for data transmission. This fixed the spin axis of the spacecraft so that the detector basically scanned the anti-Earth hemisphere. In addition, due to the orbital motion of Jupiter about the Sun, the geometry for dust detection with the dust instrument gradually changed with time, leading to the non-detectability of dust particles in the close vicinity of the Galilean moons after mid-1999. For this reason, ejecta particles were measurable during ten close Galileo flybys at Europa out of 11 flybys in total. No data could be collected during two of these encounters due to spacecraft anomalies (safings) so that data sets from eight Europa flybys are available (E4, E6, E11, E12, E14, E15, E17, E19; see also Tab II). The labels of the encounters are: the first letter of the satellite encountered by Galileo plus the number of Galileo’s orbit about Jupiter.

In Fig. 2 we show the impact direction (rotation angle) of the dust particles detected within about 2 h around closest approach to Europa whose complete set of measured impact parameters has been transmitted to Earth. During most flybys, particle impacts with  $180^\circ < \Theta < 360^\circ$  were concentrated towards Europa. This is most obvious during encounters E4, E11, E12 and E19. Most of these impacts were detected at altitudes below  $3 R_E$  ( $R_E$  is the Europa radius, see Table I).

To analyse the impact direction of the dust grains onto the detector we assumed that the speed of dust relative to Europa in the vicinity of the moon is low compared to Galileo’s flyby speed. Thus, the approach direction of the dust for an observer moving with the spacecraft is more or less parallel to the velocity vector of Europa relative to the spacecraft (the so-called ram direction). Since the orbital planes of Europa and Galileo about Jupiter coincide to within a few degrees, such particles approached the detector from a direction corresponding to  $\approx 270^\circ$  rotation angle during all eight encounters. Rotation angles of about  $90^\circ$  are opposite to the direction towards Europa. With the sensor field of view of  $140^\circ$ , particles detected with rotation angles  $180^\circ < \Theta < 360^\circ$  are compatible with an origin from Europa itself. In the following we will call them Europa particles. This detection

geometry is very similar to the one at the majority of the Ganymede flybys (Krüger et al., 2000).

**Insert Figure 2**

The direction from which the Jovian dust stream particles were observed varied during Galileo’s path through the Jovian system: when Galileo approached the inner Jovian system, rotation angles around  $270^\circ$  were observed. Between 1996 and early 1999 (the time span considered here) the rotation angle shifted to  $90^\circ$  shortly before Galileo’s closest approach to Jupiter and the stream particles approached from this direction on the outbound portion of the spacecraft trajectory. Therefore, depending on when an individual satellite flyby occurred, stream particles approached the sensor from one or the other direction. In the cases of the Europa flybys considered here, the stream particles approached from rotation angles  $0^\circ < \Theta < 180^\circ$  (*i.e.* opposite to that of the Europa particles) or stream particle impacts had already ceased because of the unfavourable detection geometry. It should be emphasized that during most of these eight Europa encounters more impacts were detected from the Europa direction than from the direction from which stream particles were to be expected. Only between zero and two impacts from the direction of the stream particles occurred during six encounters. Only encounters E6 and E17 showed the same number of impacts from  $0^\circ < \Theta < 180^\circ$  (stream particles) as from the opposite direction (Europa particles). The statistics of particle detections is given in Table II.

**Insert Table II**

A total number of 64 Europa particles have been identified below  $8 R_E$  altitude during these eight encounters purely by their impact direction (Table II). For our further analysis we use a cut-off altitude of  $8 R_E$  because this is close to the extension of Europa’s Hill sphere (Table I). We can minimize the potential contamination by particles belonging to other Jovian dust populations this way (see Sect. 3.1.3 for a discussion of their impact rates). For instance, a cut-off altitude of  $10 R_E$  would increase the number of grains classified as Europa particles by only five.

For some flybys, the numbers of identified Europa particles are lower limits to the true numbers of detected grains because the complete set of parameters measured upon impact could be transmitted to Earth for only a fraction of all impacts (column 9 of Table II). At E14, E15 and E19, however, the complete set of parameters was transmitted for all impacts within 2 h around closest approach.

In Table II (columns 7 and 8) we compare the number of Europa particles with the number of all events (dust plus noise) detected by the instrument below  $8 R_E$  and from a direction  $180^\circ < \Theta < 360^\circ$ . This shows that the noise contribution to the total number of detected events in this altitude range is between 0 and 60% with an average of 23% (17 out of 81 events are classified as noise). Although Europa orbits Jupiter in the region where high noise rates occurred, the total number of noise events in the data set is relatively small. A plot similar to Fig. 2 but with all detected events (column 8 of Table II) also shows dust concentrations at the Europa closest approaches so that the derived densities would also peak towards the satellite (Sect. 3.1.3). Hence, our conclusion that the dust impacts are concentrated towards the surface of Europa does not depend upon the applied noise removal algorithm.

We will come back to the noise problem in Sect. 3.1.3 where we will determine the spatial distribution of dust surrounding Europa. For our analysis of the Europa dust cloud we will use class 3 and noise-removed class 2 data. It should be noted that there is no physical difference between dust impacts categorised into class 2 and class 3.

### 3.1.2 Impact velocity

In Fig. 3 we show the velocity distribution of the Europa particles whose impact velocity has been determined with a velocity error factor  $VEF < 6$  (Grün et al., 1995). 53 particles fulfill this criterion. During all eight encounters of Galileo with Europa, the flyby velocity was close to  $6 \text{ km s}^{-1}$  (Table II), well above the detection threshold of the dust instrument for micrometer-sized grains at  $2 \text{ km s}^{-1}$ . We can separate two subsets of particles from their velocity distribution, similar to the measurements at Ganymede: the Jovian stream particles with velocities typically above  $10 \text{ km s}^{-1}$  and the slower Europa particles. The mean velocity of the 53 Europa particles in Fig. 3 is  $5.5 \pm 3.5 \text{ km s}^{-1}$  ( $1\sigma$ ). Given a typical uncertainty for an individual velocity measurement of a factor of two, this value is in good agreement with the velocity of Galileo relative to Europa.

**Insert Figure 3**

The velocity measurements – like the measurements at Ganymede – are in agreement with dust particles belonging to a dust cloud of Europa. They confirm that the empirical velocity calibration of the dust instrument can be applied to the relatively slow ejecta particles, although the calibration is wrong for the much smaller and faster Jovian dust stream particles. This result also confirms that the calibrated impact velocities can be used to identify particles belonging to a dust cloud when such grains cannot be identified by their impact direction. This will be applied to the data obtained in the vicinity of Callisto in Sect. 3.2.2. It should be emphasized that the two velocity distributions in Fig. 3 overlap, leading to some ambiguity in the identification of individual grains. Hence, the velocity criterion can only be applied to a statistically large data set.

In Fig. 2 we have marked particles according to their calibrated velocities: those with impact speeds below  $10 \text{ km s}^{-1}$  are shown as circles, faster grains as crosses. During seven Europa encounters of Galileo, the majority of particles with  $180^\circ \leq \Theta \leq 360^\circ$  had impact speeds below  $10 \text{ km s}^{-1}$ , consistent with a particle origin from Europa. Thus, for these seven flybys the identification of cloud particles with the velocity criterion is in agreement with the identification by the impact direction alone. Only the E19 encounter had 50% of particles (5 out of 10) with higher calibrated impact speeds so that the majority of grains would be classified as stream particles and be rejected if the impact direction were not applicable as the main identification parameter. Most of the particles detected at E19 with impact speeds above  $10 \text{ km s}^{-1}$  (4 out of 6 particles with  $0^\circ \leq \Theta \leq 360^\circ$ ), however, have a velocity error factor  $VEF > 6$ , which makes their speed calibration very uncertain, anyway. To summarize, the identification of Europa particles from their impact direction and impact speed is quite reliable for all eight Europa encounters.

### 3.1.3 Impact rate and number density

With 64 complete data sets of particles detected during eight Europa encounters we can calculate the dust impact rate in the close vicinity of this moon (Fig. 4). We have defined distance bins equally spaced on a logarithmic scale. Then we divided the number of particle impacts in each bin for which the complete set of measured impact parameters has been transmitted to Earth by the time Galileo has spent in that bin (dotted lines). Finally, to correct for incomplete data transmission (Sec. 2.1), we have multiplied the impact rate bin by bin with the ratio between the number of counted particles and the number of particles for which the complete data set has been transmitted. These corrected impact rates are shown as solid lines.

**Insert Figure 4**

Figure 4 shows that for those Europa encounters where the number of detections is sufficiently large (at least ten particles; E4, E11, E12 and E19) the impact rate clearly increases towards Europa. This implies a concentration of dust particles at Europa. It was already obvious from Fig. 2 and confirms the earlier results of a dust concentration at Ganymede (Krüger et al., 2000). On the other hand, at the remaining four encounters, the number of detections is so low that no statistically meaningful radial profile can be derived although the data are also compatible with particle concentrations at Europa. It should be noted that the correction for incomplete transmission is small in all bins and does not significantly affect the slopes of the power law fits. The slopes derived with correction for incomplete transmission are in the range  $-1.4$  to  $-2.7$  (Table II). This is somewhat flatter than the most reliable slopes obtained for Ganymede (Krüger et al., 2000).

An important question arises: is the slope of the dust distribution at Europa truly flatter than that at Ganymede or is it an artefact caused by the measurement process? Two effects may cause a flattening of the slope: 1) a background of dust particles in jovian space; and 2) incomplete removal of noise events by our noise removal technique. Both would lead to an artificial flattening of the derived dust impact rate profile.

To analyze the first hypothesis – a background dust population – we consider the complete data set of Galileo dust measurements in the Jovian system: the dust instrument has detected a number of micrometer-sized particles mostly in the region between the Galilean moons (Grün et al., 1998). At least two populations of grains can be distinguished: particles on bound prograde orbits about Jupiter and a population on retrograde orbits (Colwell et al., 1998b,a; Thiessenhusen et al., 2000; Krivov et al., 2002a). Depending on the detection geometry of the dust instrument during a specific orbit of Galileo about Jupiter, impact rates of particles from both populations taken together were up to six per day in the region of Europa (Thiessenhusen et al., 2000, their Fig. 10). Considering that one Galileo passage through Europa’s Hill sphere (Table I) lasted about 75 min, only one dust impact from these populations has to be expected every third Europa flyby. We therefore conclude that a contamination by particles on jovian orbits is negligible for our analysis of the Europa dust cloud.

A potential contamination caused by such grains would be even smaller at Ganymede and Callisto because their number density decreases further away from Jupiter.

In order to check the second possibility – incomplete removal of noise events from the data set – we use an alternative approach to calculate noise-free dust impact rates. The noise removal algorithm applied so far determines whether each individual class 2 event is most likely a true dust impact or a noise event. Instead, we calculate the average noise rate measured with the dust instrument and subtract it from the total counted rate to obtain the dust impact rate. We have first calculated the total event rate of dust impacts *plus noise* with the same technique as before, *i.e.* from the complete data sets, without applying our noise-removal scheme. This gives somewhat flatter power law slopes than those derived for the noise-removed data set (between  $-1$  and  $-2$ ). We have then calculated the fraction of noise events in the class 2 accumulator data with our noise identification scheme during a one-day interval centered around each Europa flyby and calculated the rate of noise events in the counter data by multiplying the total counted rate with the fraction of noise events. Typical noise rates are between 0.04 and 0.1 per minute. We have then subtracted this noise rate from the total event rate obtained from the entire data sets. The resulting radial density profiles have power law slopes between  $-2$  and  $-4$ . The theoretically expected value is about  $-2.5$ , or more precisely it is steeper than  $-2.5$  for  $r \lesssim 5 R_{\text{sat}}$  (bound grains dominate) and it becomes flatter, between  $-2.5$  and  $-2$  (escaping grains dominate), farther out (Krivov et al., 2003). Thus, we conclude that the observed radial density profiles which are somewhat flatter than the expected values may be due to incomplete noise removal.

We do not investigate variations of the slopes between individual encounters because of the large statistical uncertainties and the potential unrecognised noise contamination of the data. Spatial variations with respect to the flyby position relative to the satellite will be addressed in a future investigation.

**Insert Figure 5**

With the impact rate profiles derived for the individual Europa encounters we can now calculate the spatial density of dust in the environment of this satellite. We first divide bin by bin the impact rate by the spin-averaged detector area to obtain fluxes ( $\text{m}^{-2}\text{s}^{-1}$ ). Then we divide these fluxes by the mean impact velocity (spacecraft velocity relative to the moon) for a given flyby. This results in mean number densities ( $\text{m}^{-3}$ ) in the various distance bins. Note that the slope of the number density is the same as that of the impact rate, because both the spin-averaged detector area and the mean impact velocity are assumed to be constant (independent of distance) for any individual flyby. The result is shown in Fig. 5. The number densities show a clear increase towards Europa and the average slope is  $-2.02 \pm 0.63$ . It is remarkable that the variation in the derived number densities from encounter to encounter is relatively small. Since the closest approaches of Galileo at Europa occurred at different longitudes and latitudes of Europa, it indicates that the dust distribution around this moon does not show strong spatial or temporal variations.

We have also checked alternatives for the origin of the dust impacts detected in the close vicinity of the Galilean satellites other than the impact-ejection mechanism (Krüger et al., 2000). Gravitational capture of the grains by the satellites can be dynamically ruled out. Electromagnetic interactions seem to be too weak, in particular at Europa and Callisto which do not have their own magnetic fields. Although the geysers on Io are the most likely source for the Jovian dust stream particles, no geyser activity has been observed on the other Galilean moons. The most plausible explanation for the origin of the dust grains was continuous bombardment of the satellites by interplanetary micrometeoroids.

In this work we assume spherical symmetry of the clouds which is supported by our measurements: passages of Galileo at different latitudes and longitudes of the moons did not reveal strong asymmetries in the dust distribution, except, possibly, at Callisto (see Sect. 3.2.3). This implies a spherical structure of the dust distribution surrounding the satellites. Of course, it does not rule out the existence of asymmetries in the dust density which will be investigated in the future (Sremčević et al., 2003).

We now look at the number density profile expected from theory. Krivov et al. (2003) developed a model of a spherically symmetric, stationary dust cloud around a satellite, maintained by impacts of interplanetary micrometeoroids. To the first approximation, the number density of dust grains ejected into ballistic orbits, which dominate the cloud at distances of several satellite radii, is

$$n_{\text{bound}}(x) \propto x^{-5/2}, \quad (2)$$

where  $x \equiv r/R_{\text{sat}}$  is the distance measured in satellite radii. The contribution of escaping grains into the cloud is somewhat shallower:

$$n_{\text{unbound}}(x) \propto x^{-2} \quad (3)$$

which slightly flattens the overall radial profile at larger distances from the moon, closer to its Hill's sphere.

Krivov et al. (2003) have also constructed an algorithm to calculate the proportionality factors in Eqs. (2)–(3). The algorithm implies a chain of estimates: for the mass flux and typical speed of projectiles, for gravitational focussing of impactors by Jupiter, for the ejecta yield, ejecta mass and velocity distributions, etc. The values of the model parameters (both assumed and derived) for Europa are given in Table III. Other parameters that have the same values for all Galilean satellites, are: slope of cumulative ejecta mass distribution  $\alpha = 0.83$ , maximum mass of an ejected fragment  $M_{\text{max}} = 10^{-5}$  g, opening angle of cone into which particles are ejected  $\psi_0 = 90^\circ$ . For a detailed description of the parameters, the reader is referred to the original paper. We note that the model calculates number densities of particles with masses above the detection threshold of the Galileo dust detector. As the threshold is speed-dependent, the number densities are computed separately for each Galileo flyby, and the results for specific flybys generally differ even for the same moon and the same distance. A strong advantage of this approach is that it enables direct comparison of the number densities predicted by the model with those derived from the measurements.

Using this model for Europa, we obtained theoretical curves superimposed on the data points in

Fig. 5. A comparison between the number densities derived from the Galileo measurements and those computed with the model will be given in Sect. 4.

Insert Table III

### 3.1.4 Mass distribution

The charge released by an impact of a dust particle onto the detector target depends on the mass and the velocity of the grain (Equ. 1). In particular, to calculate the particle mass one has to know its impact velocity. The calibration of velocity and mass from the measured charge rise times and charge amplitudes is usually performed based on laboratory measurements obtained at a dust accelerator.

In Fig. 6 we show the mass distribution of the particles from all eight Europa flybys for which the velocity could be reliably determined ( $VEF < 6$ ; 53 particles in total). In the upper panel the complete instrument calibration has been used to obtain particle speed and mass. With this method the uncertainty of the impact velocity is typically a factor of 2 and that of the mass is a factor of 10.

Insert Figure 6

The dust detector has a velocity-dependent detection threshold (Grün et al., 1995). The threshold for particles approaching with  $6 \text{ km s}^{-1}$  is shown as a dashed line. The mass distribution is incomplete around this value.

The mass distribution is also affected by the low data transmission capability of Galileo and the data storage scheme in the instrument memory. As a result, nearly all data sets lost are in the lowest amplitude range AR1 which — for particle velocities of about  $6 \text{ km s}^{-1}$  — corresponds to the mass range below  $\sim 3 \times 10^{-15} \text{ kg}$ . If we assume that the lost particles are equally distributed over the mass bins below this value, the maximum of the mass distribution is artificially too low by less than a factor of 1.2. Thus, incomplete data transmission does not significantly affect the mass distribution for Europa particles.

If the individual impact velocities of dust particles were known with a higher accuracy than the typical factor of 2 uncertainty from the instrument calibration, the uncertainty in the mass determination could be improved. The measured mean impact velocities of Europa particles are close to the velocity of Galileo relative to Europa during the individual encounters (Table II). We therefore assume the latter ones as the particles' impact velocities and show the recalculated particle mass in the lower panel of Fig. 6. The width of the mass distribution is significantly smaller than that derived from the calibrated impact velocities. This method has also been successfully applied to calculate the size distribution of Ganymede ejecta particles (Krüger et al., 2000) and interstellar dust particles measured with Galileo and Ulysses (Landgraf et al., 2000).

The mean mass of the Europa particles is  $9.0 \times 10^{-15} \text{ kg}$ . Assuming spherical particles with a density

of  $1 \text{ g cm}^{-3}$  – the density of water ice – this corresponds to a particle radius of  $\approx 1 \mu\text{m}$ .

Degradation of the dust instrument caused by the high radiation dosages in the Jovian magnetosphere lead to shifts of the calibrated masses and impact speeds of the dust particles. All data collected after mid-1997 are affected by this shift, the later in the mission the data were collected, the stronger the shift. For our Europa measurements this means that masses are too low by a factor of about 1.5 beginning with the E11 encounter. We have corrected the calibrated masses for these data sets and constructed a corrected mass distribution (solid histogram in the bottom panel of Fig. 6). Since we have taken the speed of Galileo relative to Europa as the impact speed of the particles, we need to correct the masses only. The shift in the velocity calibration caused by the instrument degradation does not affect this mass distribution. The resulting mean mass of the Europa particles is  $1.3 \times 10^{-14} \text{ kg}$ . It should be emphasized that the shift in the velocity calibration does not affect the identification of the Europa particles because the particles at the Europa encounters have been identified by their impact direction alone, without using the impact speed as an additional criterion.

## 3.2 Callisto

### 3.2.1 Impact direction

During Galileo’s prime mission about Jupiter in 1996 and 1997 the spacecraft had three close flybys at Callisto (C3, C9, C10). The spacecraft orientation during these encounters allowed the detection of ejecta cloud particles close to Callisto. During all Callisto flybys after mid-1999 the spacecraft orientation prevented the detection of ejecta cloud particles so that the measurements at Callisto are restricted to these three encounters. Unfortunately, all three of them occurred on the portion of the Galileo trajectory inbound to Jupiter where Jupiter stream particles and potential ejecta particles from Callisto approached the dust sensor from the same direction ( $180^\circ \leq \Theta \leq 360^\circ$ ; Sect. 3.1.1). This is shown in Fig. 7: almost the entire number of dust impacts measured close to Callisto occurred from this direction. Thus, Callisto particles could not be uniquely identified by their impact direction alone, and we had to use the impact velocity as an additional criterion to identify them.

**Insert Figure 7**

The analysis of the ejecta particles detected at Europa (Sect. 3.1.2) and Ganymede (Krüger et al., 2000) showed that – on average – stream particles and ejecta cloud particles occupy different regimes in calibrated impact speed: cloud particles have typical speeds below  $10 \text{ km s}^{-1}$  which are on average very close to the encounter velocity of Galileo with the satellite, whereas stream particles have significantly higher calibrated speeds. This has been successfully applied to identify Ganymede cloud particles from Galileo’s G8 encounter at Ganymede. We apply the same velocity criterion here to separate Callisto particles from the dust streams. The numbers of Callisto particles identified this way are listed in Table II for each orbit. The total number of Callisto particles from all three encounters is 35.

Only particles detected at altitude below  $6 R_C$  are considered for further analysis in order to minimize the contamination by stream particles. The analysis of the Europa and Ganymede data showed that a few stream particles have calibrated velocities below  $10 \text{ km s}^{-1}$  and would erroneously be classified as Callisto particles (Fig. 7). Most cloud particle impacts at Europa and Ganymede occurred below an altitude of about  $6 R_{\text{sat}}$  (Fig. 2 and (Krüger et al., 2000)) so that the inclusion of particles detected further away would increase the probability that the particles are actually stream particles rather than dust cloud particles. An apparent concentration of stream particle impacts within  $3 R_C$  altitude at C3 and within  $5 R_C$  at C10 (Fig. 7) is due to a higher data transmission rate of Galileo in these periods (Krüger et al., 2001).

Callisto orbits Jupiter outside the region within  $15 R_J$  where the high noise rates occurred. Thus, a potential noise contamination of the Callisto data is expected to be very low. For our analysis of the Callisto dust cloud we will use class 3 and class 2 data without noise removal.

### 3.2.2 Impact velocity

A total number of 35 Callisto particles have been identified by their calibrated impact velocity below  $10 \text{ km s}^{-1}$  and below an altitude of  $6 R_C$ . Their mean impact velocity is  $6.4 \pm 2.1 \text{ km s}^{-1}$  ( $1 \sigma$ ). This value is artificially too low because the velocity distribution is cut off at  $10 \text{ km s}^{-1}$ . The average flyby speed of Galileo at Callisto was  $8.1 \text{ km s}^{-1}$  and both speeds agree within  $1 \sigma$ . The velocity distribution of the Callisto particles is shown in Fig. 8.

Insert Figure 8

Degradation of the dust instrument electronics does not significantly affect the impact velocities of the particles because most the Callisto encounters occurred relatively early during the Galileo mission. In particular, the identification of Callisto particles via their impact speed is not affected.

### 3.2.3 Impact rate and number density

With Callisto particles from all three Callisto encounters identified by their impact speed and impact direction, we can construct the radial profile of the dust impact rate in the same way as we did for the Europa flybys before. This is done in Fig. 9. For the C3 and C10 encounters the impact rate increased towards Callisto. At C9 the number of detected particles was only three. The derived radial profile — although being very uncertain — is compatible with an increase towards Ganymede. We conclude that the dust impact rates detected at Callisto are compatible with a dust concentration surrounding this moon.

Insert Figure 9

In Fig. 10 we show the number densities for Callisto derived from the radial profiles of the impact

rate. The data from the individual flybys show an increase towards the surface of the moon. The number densities derived from the three flybys show a large variation from flyby to flyby, much larger than those for Europa. In particular, the number densities derived from the C9 data are very low. Possible reasons for this variation will be discussed in Sect. 4.

In the same figure, the superimposed curves show the number density profile calculated with the model (Krivov et al., 2003) and parameters listed in Table III. A comparison between the data and the model will be given in Sect. 4.

Insert Figure 10

### 3.2.4 Mass distribution

The mass distribution for the 35 Callisto particles with  $VEF < 6$  is shown in Fig. 11. As for Europa, we show the mass distribution with the calibrated impact velocities (upper panel) and that obtained by applying the velocity of Galileo relative to Callisto (bottom panel). Here the detection threshold is  $8 \text{ km s}^{-1}$ , and the mass distribution is incomplete around the threshold. Again, the mass distribution is incomplete in the bins below about  $10^{-15} \text{ kg}$  due to incomplete data transmission and the maximum of the mass distribution may be artificially too low by up to a factor of 1.3.

Insert Figure 11

The mean calibrated mass of the Callisto particles is  $3.7 \times 10^{-16} \text{ kg}$ , which is an order of magnitude lower than the value derived for the Europa cloud particles. Again, assuming spherical particles with a density of  $1 \text{ g cm}^{-3}$ , this corresponds to a particle radius of  $0.5 \mu\text{m}$ . We have also corrected the masses of the particles for instrument degradation and constructed a corrected mass distribution (solid histogram in the bottom panel of Fig. 11). The corrected mean mass of the Callisto particles is  $5.2 \times 10^{-16} \text{ kg}$ .

## 3.3 Io

### 3.3.1 Impact direction

Galileo had a total of seven flybys at Io but only the initial one in December 1995 (I0; the orbit notation is I "zero") had a favourable detection geometry. During the other flybys at this satellite which occurred after mid-1999 the sensor orientation prevented the detection of ejecta dust particles. Figure 12 shows the sensor orientation at particle impact at the I0 encounter. The bottom panel shows class 3 and noise-removed class 2 data (only four impacts).

The noise identification criteria applied to the Europa data have been developed for the spatial region outside  $10 R_J$ . The I0 data, however, have been collected closer to Jupiter at  $6 R_J$  where the noise

characteristics may have been different (Krüger et al., 1999c). We therefore show the full data set of classes 1 to 3 in the top panel of Fig. 12. The noise fraction in class 2 derived with the algorithm for secondary ejecta grains is about 80%. The complete class 2 data set also shows a concentration of grains towards Io. Therefore, the noise rejection algorithm may be too restrictive, thus rejecting too many events. Class 1 events, which are usually classified as noise in the Jovian environment, show an interesting behaviour: the impacts cluster at rotation angles  $0 \leq \Theta \leq 180^\circ$ . This direction is compatible with the approach direction of plasma particles in the Io torus.

A few days before the flyby at Io, the channeltron high voltage was decreased and the charge detection thresholds were raised (Grün et al., 1996; Krüger et al., 1999b) to reduce the instrument sensitivity in the high radiation environment of the inner Jovian magnetosphere. This reduced the instrument sensitivity for class 3 impacts. Those impacts, however, that did not generate enough charge to become class 3 events should have shown up as class 2 impacts. Unfortunately, class 2 is contaminated with noise so that the identification of these particles is ambiguous. Fortunately, only a small fraction of the data sets of particles was lost due to incomplete data transmission (Table II).

**Insert Figure 12**

Figure 12 shows four particles within an altitude of about  $6 R_I$  (the Hill sphere of Io). Two of these particles approached the detector from a direction  $\Theta \approx 270^\circ$ . The other two particles were detected when the dust detector pointed  $\approx 90^\circ$  away from this direction. A check of the approach direction of potential Io particles revealed that all four particles are compatible with an Io origin: the approach direction of Io particles as seen from Galileo was so close to the spin axis of the spacecraft (direction opposite to antenna axis) that they were detectable at almost all rotation angles (Krüger et al., 1999c). We therefore consider all four particles as probable Io particles. Only one of these impacts occurred in ion amplitude range AR1, two were detected in AR2 and one in AR3. Io dust stream particles were detected in AR1 only (Grün et al., 1998) so that the identified particles were unlikely stream particles. In addition, the impact rate of stream particles was reduced in the inner Jovian system because of reduced impact speeds (Graps, 2001).

### 3.3.2 Impact velocity

The total number of identified potential ejecta particles from Io is only four. With this very low number of detections no reasonable velocity distribution can be constructed. We can, however, still check whether the average particle velocity is compatible with the hypothesis that the particles are basically at rest with respect to Io. The velocity of Galileo relative to Io at the IO encounter was  $15 \text{ km s}^{-1}$ . The averaged particle speed derived for the four particles is  $10.3 \pm 8.4 \text{ km s}^{-1}$ . Although one has to keep in mind that the statistical uncertainty of this value is very large, it is compatible with particles being bound to Io.

### 3.3.3 Impact rate and number density

The dust impact rate at Io derived from the four identified Io particles is shown in Fig. 13. It shows a slight concentration towards Io. One has to keep in mind, however, that the radial profile of the impact rate is very uncertain because of the small number of dust detections in the close vicinity of this moon.

Insert Figure 13

Insert Figure 14

The number density of dust in the close vicinity of Io derived from the impact rate profiles is shown in Fig. 14. For comparison we show the data points for the noise-removed data set (solid lines) and for the complete class 2 and class 3 data set. The curves in the same figure depict the number density profile calculated with the model (Krivov et al., 2003) and parameters listed in Table III. A comparison between the data and the model will be given in Sect. 4.

### 3.3.4 Mass distribution

No attempt has been made to construct a mass distribution because of the small number of detections at this moon. The mean mass of the particles taking the speed of Galileo relative to Io as the impact speed is  $8.5 \times 10^{-16}$  kg. Note that this value is not affected by the instrument degradation because this Io flyby occurred at the beginning of Galileo's Jupiter mission.

## 4 Comparison of the dust clouds surrounding the Galilean moons

In the previous section we have analyzed the dust impacts detected in the circumsatellite dust clouds individually for Io, Europa and Callisto. The dust cloud of Ganymede has been investigated in an earlier publication (Krüger et al., 2000). For each of the four moons we have identified impacts of probable ejecta cloud particles in the Galileo dust data set, determined their impact speeds and mass distributions and have derived impact rate and number density profiles. We now take the data sets for all four moons together to compare the properties of their surrounding dust clouds.

### 4.1 Mass distribution

The mass distribution of the grains allows a simple check for the compatibility of the data with the hypothesis of the impact origin of the detected particles. We took the mass distributions for Europa, Callisto and Ganymede (Fig. 6, Fig. 11 and (Krüger et al., 2000)) and show linear fits to the cumulative distributions in Fig. 15. The slopes of the cumulative mass distributions assuming

Galileo’s velocity relative to each moon as the particle impact speed are given in Table IV. Only one data point is shown for Io because of the scarcity of the data. For the three other moons the slopes are in the range between 0.58 and 0.86, which is in good agreement with the typical slopes one expects for impact ejecta ( $0.5 \lesssim \alpha \lesssim 1.0$ ; see, *e.g.*, Koschny and Grün (2001)). It should be emphasized that even though the statistical uncertainties in the data sets are relatively large because of the small number of detections, the slopes derived for the three moons do not differ very much. The slopes derived for the mass distributions taking the calibrated impact speeds are in the range 0.5 – 0.6 and are thus even closer together, although they are flatter than those derived with the spacecraft speed relative to the moon.

It should be noted that the mass distributions of dust around Ganymede and Callisto agree very well (0.82 vs. 0.86) whereas the one for Europa is somewhat flatter (0.58). This might reflect differences in surface properties of the satellites: for instance, flatter mass distributions are typical of looser targets than of consolidated ones (see, *e.g.*, Koschny and Grün, 2001, and references therein).

**Insert Figure 15**

**Insert Table IV**

## 4.2 Number densities

The number densities derived for all four Galilean moons are shown in Fig. 16. Straight lines are least squares fits to the data for each moon. We list the slopes of these curves, which are averages of slopes for individual flybys at each moon, in Table IV (col. 8). The average slopes for each moon are between  $-1.6$  for Callisto and  $-2.8$  for Ganymede, with Europa being in between ( $-2.0$ ). The very uncertain slope for the Io data ( $-2.0$ ) is close to the Europa value. The Ganymede data show the steepest slope but also the largest uncertainty. This is mainly caused by the incomplete data transmission which mostly affected the G2 and G8 measurements. The incompleteness affects the error via  $\propto (N \pm \sqrt{N}) \times \text{correction}$ , therefore giving larger limits compared to the 100% transmission case.

Altogether, the slopes are roughly consistent with the one predicted in the framework of the spherically-symmetric cloud model (Krivov et al., 2003), between  $-2.0$  and  $-2.5$  [see Eqs. (2)–(3)]. Only the slope derived for Callisto is somewhat flatter. A study of possible asymmetry effects in the clouds has shown that this “reference” slope may be substantially flatter or steeper, depending on the flyby geometry and the position of the satellite in its orbit at the time of flyby (Sremčević et al., 2003). This may account for a tangible scatter in the slopes that we derived from the data.

The measured absolute number densities of all four clouds at a given distance (measured in satellite radii) are similar — see Fig. 16. It is important to compare this result with the theory. The absolute number density of a dust cloud at a given distance from a satellite should depend in a non-trivial way

on a number of factors: mass of the moon, its planetocentric distance (through a distance-dependent gravitational focussing of the impactor flux), as well as the satellite surface properties. All these dependences are taken into account in the model which was confined, however, to a solid ice-silicate surface (Krivov et al., 2003). The number densities of the clouds around Europa, Ganymede and Callisto, computed with the model, turned out to be within a factor of several from each other (most notably, larger yields  $Y$  for closer-in satellites are compensated by lower ejecta speeds  $u_0$ , because of an energy conservation requirement used in the model). The number densities of these three clouds are consistent with the densities derived from the data. Not so for the Io cloud: the same model (Krivov et al., 2003) predicts a much higher dust number density (mostly because of the larger flyby speed at Io, resulting in a possibility of detecting much smaller dust grains compared to the other Galileans). The number density in the Io cloud predicted by the model is at least an order of magnitude higher than observed. This could be due to the scarcity of the Io data (4 individual dust impacts only). Alternatively, this may be a real effect, caused by different surface properties of Io (volcanic deposits and condensed gases like  $SO_2$  frost) compared to the other three Galilean moons (presumably “solid” ice with some contamination by non-volatile materials). Such a view seems to be indirectly supported by our preliminary analysis of the dust environment between the orbits of Io and Europa (work in progress): the density of the “Galilean ring” (Krivov et al., 2002a) does not seem to increase from the Europa orbit towards Jupiter, which might be compatible with Io being a weaker source of ejecta than it would be, if it were similar in surface properties to the other Galilean satellites.

**Insert Figure 16**

A comparison of data from different flybys at the same moon shows that for Europa the derived dust densities do not vary significantly from flyby to flyby. This indicates little or no temporal variation and/or dust density variation between the leading and the trailing side of this moon with respect to the field of impactors. On the other hand, the three Callisto flybys showed a significant variation by more than an order of magnitude between the C9 and the C10 flybys. For Ganymede, the G2 and G8 flybys showed somewhat larger number densities than the G1 and G7 flybys. The former, however, have the largest uncertainties because of incomplete data transmission and particle identification via the impact speed criterion. At present, it is not clear whether the differences between the data from different flybys of Callisto and Ganymede can be attributed to asymmetries in the circumsatellite dust clouds modelled in Sremčević et al. (2003). A comparison between the data and theory is hampered by poorly known directionality of impactors in the vicinity of Jupiter. This issue will be the subject of a future investigation.

### 4.3 Grain velocities in the clouds

The theoretical models of dust clouds predict that, on average, the constituent particles should have substantial velocities with respect to their parent satellites. Based on Krivov et al. (2003) formulas, about 40–50% of the grains at distances from 2 to 8  $R_{\text{sat}}$  in the Ganymede and Callisto clouds should

be faster than  $2\text{ km s}^{-1}$ . For Europa the fraction is 30–40%.

The question that we address now is: can we find indications in the data that some grains have appreciable velocities relative to the respective moon? The most natural way would be to look at possible deviations of the actual impact speeds from the mean value, equal to the spacecraft speed with respect to the satellite. Unfortunately, this is not possible: as we have seen (Figs. 3 and 8), the instrument calibration is by far not accurate enough to do that. Another possibility would be to look at the impact directions, *i.e.* at the rotation angles of impacts. For most of the flybys the cloud particles, if they were at rest with respect to the moon, could only be detected in the rotation angle range  $\Theta = 270^\circ \pm x$ , where the semi-width  $x$  of the detectability range is a (known) function of the FOV opening angle and the angle between the Galileo ram direction and its spin axis,  $\beta$ . The semi-width  $x$  is  $180^\circ$  for  $\beta \leq 10^\circ$  and decreases to  $67^\circ$  at  $\beta = 90^\circ$ . Should a particle, which we identify as a cloud particle, have had a  $\Theta$  value somewhat outside the range  $\Theta = 270^\circ \pm x$ , this would be an indication that the particle had an appreciable velocity, so that the impact velocity deviated markedly from the anti-ram direction.

One should not expect the number of such events to be high: even very fast grains can only show up in this test if the direction of their velocity vector is appropriate, and only for some flyby geometries. We have checked all cloud particles and found four individual impacts of this kind: one in G7, one in E11 and two in E12.

#### 4.4 Mass budget

As was the case for Ganymede earlier (Krüger et al., 2000), we give some general estimates concerning the mass budget of the dust clouds of the other Galilean moons as derived from the model (Krivov et al., 2003). The results, including new estimates for Ganymede, are collected in Table V. Note that these are only crude estimates which are uncertain by at least one order of magnitude, perhaps even more. The expected steady-state masses of the clouds range from about 10 tons for Callisto to about 200 tons for Io; the Io cloud may, however, be lighter — see discussion in Sect. 4.2. Interestingly, the mass injection rate of the material into circumjovian space is similar for all four moons and is, in turn, comparable to the mass flux of impactors onto respective satellites,  $\sim 100\text{ g s}^{-1}$ . This means that each satellite “redirects” nearly as much dust into the circumplanetary space as it receives from the interplanetary one. Of course, the mass/size and velocity distributions of the “incoming” and “outgoing” matter are generally quite different.

**Insert Table V**

## 5 Conclusions

We have examined the dust impacts registered by the Galileo dust detector in the immediate vicinity of Io, Europa and Callisto during a total of 12 flybys at these Jovian moons. By analyzing impact directions and velocities and the mass distribution, as well as spatial locations of the dust impacts in comparison with model predictions (Krivov et al., 2003), we have shown that the particles originated from the moons. Our analysis technique was similar to an earlier investigation of dust data collected at Ganymede (Krüger et al., 2000). The dust impacts recorded at all four moons are compatible with impact debris produced by hypervelocity impacts onto the surfaces of these moons. For the icy moons Europa, Ganymede and Callisto, the mass distributions of the detected grains, as well as the spatial dust densities derived from the measurements are in fairly good agreement with the predictions from the model of hypervelocity impacts of interplanetary dust particles (IDPs), assuming contemporary models of IDP flux at a heliocentric distance of Jupiter and a low-temperature ice-silicate target. For Io, the number of dust detections is too small to derive a reliable mass distribution. The number density obtained for this moon is more than an order of magnitude lower than predicted by the model which assumes a solid ice surface. The lack of detections may be due to a softer, fluffier surface of Io compared to the three icy Galilean moons. Io's surface is (at least partially) covered with volcanic deposits.

This work continues the analysis of the dust clouds surrounding the Galilean moons and confirms the previous scenario of ejecta dust clouds generated by hypervelocity impacts of micrometeoroids. Up to now, this had only been tested at Ganymede. Our theoretical description is based on the physical conditions in the Jovian system as well as available laboratory data of hypervelocity impacts. We have neglected any spherical asymmetries of the dust clouds surrounding the moons. To a first approximation, this is supported by the data, especially the measurements taken at Europa. On the other hand, the Callisto and possibly Ganymede measurements show a variation between different flybys which might be indicative of a leading-trailing cloud asymmetry caused by the motion of the moons through the field of impactors, as predicted by theory (Sremčević et al., 2003). This will be addressed in a future analysis.

Most of the dust ejected from the surface is launched into bound orbits and falls back to the moon. These short-lived, but continuously replenished grains form the ejecta dust clouds. A tiny fraction of impact debris is ejected at speeds sufficient to escape from the moon entirely. The ejected mass is comparable with the incoming flux of IDP impactors. The escaping grains go into orbit about Jupiter and most of them will eventually be swept up by one of the Galilean satellites. A tiny fraction of them forms a tenuous dust ring surrounding the planet (Krivov et al., 2002a). This ring is by far too tenuous to be detected optically. By the impact ejecta mechanism, moons turn out to be efficient sources for dusty planetary rings. In particular, Jupiter's gossamer ring and Saturn's E ring are thought to be maintained by ejecta particles from smaller moons which orbit their parent planets within the rings. In November 2002 Galileo traversed the gossamer ring and had a close flyby of Amalthea, one of the

small Jovian moons which orbits the planet within the ring region. The dust measurements collected during this passage may give new insights into the dynamics and feeding mechanism of this dusty ring and about the significance of small moons as sources of dust.

All celestial bodies without gaseous atmospheres (asteroids and planetary satellites of all sizes) should be surrounded by an ejecta dust cloud. The dust particles in the cloud are composed of surface material from the parent body and, hence, carry information about the surface from which they have been kicked up. Our analysis of the Galileo in-situ dust data has shown that spacecraft measurements near celestial bodies — which act as sources of dust — can be used as a new diagnostic tool to analyze the surface properties of these bodies. This is of particular interest for the Cassini mission which will investigate the Saturnian system beginning in 2004. The Cassini dust instrument will be able to measure the chemical composition of particles in the dust clouds surrounding the Saturnian moons. This way, the surface properties of the source moons can be investigated remotely. Interestingly, the in-situ dust measurements turn into a remote sensing technique where the dust instrument is used like a telescope for surface investigation.

**Acknowledgements.** The authors wish to thank Frank Spahn for many valuable discussions. This research has been supported by the German Bundesministerium für Bildung und Forschung through Deutsches Zentrum für Luft- und Raumfahrt e. V. (DLR, grants 50 QJ 9503 3 and 50 OH 0003) and by the Deutsche Forschungsgemeinschaft (DFG, grant No. Sp 384/12-3). We wish to thank the Galileo project at JPL for effective and successful mission operations.

## References

- Baguhl, M. (1993). *Identifikation von Staubeinschlägen in den Daten der Mikrometeoriden-Detektoren an Bord der Raumsonden Ulysses und Galileo*. PhD thesis, Ruprecht-Karls-Universität Heidelberg.
- Baguhl, M., Grün, E., Linkert, G., Linkert, D., and Siddique, N. (1993). Identification of ‘small’ dust impacts in the Ulysses dust detector data. *Planetary and Space Science*, 41:1085–1098.
- Burns, J. A., Showalter, M. R., Hamilton, D. P., Nicholson, P. D., de Pater, I., Ockert-Bell, M. E., and Thomas, P. C. (1999). The formation of Jupiter’s faint rings. *Science*, 284:1146–1150.
- Colwell, J. E., Horányi, M., and Grün, E. (1998a). Jupiter’s exogenic dust ring. *J. Geophys. Res.*, 103:20023–20030.
- Colwell, J. E., Horányi, M., and Grün, E. (1998b). Capture of interplanetary and interstellar dust by the Jovian magnetosphere. *Science*, 280:88–91.
- Göller, J. R. and Grün, E. (1989). Calibration of the GALILEO/ULYSSES dust detectors with different projectile materials and at varying impact angles. *Planet. Space Sci.*, 37:1197–1206.
- Graps, A. L. (2001). *Io revealed in the Jovian dust streams*. PhD thesis, Ruprecht-Karls-Universität Heidelberg.
- Graps, A. L., Grün, E., Svedhem, H., Krüger, H., Horányi, M., Heck, A., and Lammers, S. (2000). Io as a source of the Jovian dust streams. *Nature*, 405:48–50.
- Grün, E., Baguhl, M., Hamilton, D. P., Kissel, J., Linkert, D., Linkert, G., and Riemann, R. (1995). Reduction of Galileo and Ulysses dust data. *Planetary and Space Science*, 43:941–951.
- Grün, E., Fechtig, H., Hanner, M. S., Kissel, J., Lindblad, B. A., Linkert, D., Maas, D., Morfill, G. E., and Zook, H. A. (1992). The Galileo dust detector. *Space Science Reviews*, 60:317–340.
- Grün, E., Gustafson, B. E., Mann, I., Baguhl, M., Morfill, G. E., Staubach, P., A., T., and Zook, H. A. (1994). Interstellar dust in the heliosphere. *Astronomy & Astrophysics*, 286:915–924.
- Grün, E., Hamilton, D. P., Riemann, R., Dermott, S. F., Fechtig, H., Gustafson, B. A., Hanner, M. S., Heck, A., Horányi, M., Kissel, J., Kivelson, M., Krüger, H., Lindblad, B. A., Linkert, D., Linkert, G., Mann, I., McDonnell, J. A. M., Morfill, G. E., Polanskey, C., Schwehm, G. H., Srama, R., and Zook, H. A. (1996). Dust measurements during Galileo’s approach to Jupiter and Io encounter. *Science*, 274:399–401.
- Grün, E., Krüger, H., Graps, A., Hamilton, D. P., Heck, A., Linkert, G., Zook, H., Dermott, S. F., Fechtig, H., Gustafson, B., Hanner, M., Horányi, M., Kissel, J., Lindblad, B., Linkert, G., Mann, I., McDonnell, J. A. M., Morfill, G. E., Polanskey, C., Schwehm, G. H., and Srama, R. (1998). Galileo observes electromagnetically coupled dust in the Jovian magnetosphere. *J. Geophys. Res.*, 103:20011–20022.

- Grün, E., Krüger, P., Dermott, S. F., Fechtig, H., Graps, A. L., Gustafson, B. A., Hamilton, D. P., Heck, A., Horányi, M., Kissel, J., Lindblad, B. A., Linkert, D., Linkert, G., Mann, I., McDonnell, J. A. M., Morfill, G. E., Polanskey, C., Schwehm, G. H., Srama, R., and Zook, H. A. (1997). Dust measurements in the Jovian magnetosphere. *Geophysical Research Letters*, 24:2171–2174.
- Grün, E., Zook, H. A., Baguhl, M., Balogh, A., Bame, S. J., Fechtig, H., Forsyth, R., Hanner, M. S., Horányi, M., Kissel, J., Lindblad, B. A., Linkert, D., Linkert, G., Mann, I., McDonnell, J. A. M., Morfill, G. E., Phillips, J. L., Polanskey, C., Schwehm, G. H., Siddique, N., Staubach, P., Svestka, J., and Taylor, A. (1993). Discovery of Jovian dust streams and interstellar grains by the Ulysses spacecraft. *Nature*, 362:428–430.
- Hamilton, D. P. and Burns, J. A. (1994). Origin of Saturn’s E ring: Self-sustained – naturally. *Science*, 264:550–553.
- Horányi, M., Burns, J. A., and Hamilton, D. P. (1992). The dynamics of Saturn’s E ring particles. *Icarus*, 97:248–259.
- Horányi, M. and Cravens, T. E. (1996). The structure and dynamics of Jupiter’s ring. *Nature*, 381:293–298.
- Horányi, M., Morfill, G. E., and Grün, E. (1993a). Mechanism for the acceleration and ejection of dust grains from Jupiter’s magnetosphere. *Nature*, 363:144–146.
- Horányi, M., Morfill, G. E., and Grün, E. (1993b). The dusty ballerina skirt of Jupiter. *J. Geophys. Res.*, 98:21245–21251.
- Koschny, D. and Grün, E. (2001). Impacts into Ice-Silicate Mixtures: Ejecta Mass and Size Distributions. *Icarus*, 154:402–411.
- Krivov, A. V. and Hamilton, D. P. (1997). Martian dust belts: Waiting for discovery. *Icarus*, 128:335–353.
- Krivov, A. V. and Jurewicz, A. (1999). The ethereal dust envelopes of the Martian moons. *Planetary and Space Science*, 47:45–56.
- Krivov, A. V., Krüger, H., Grün, E., Thiessenhusen, K.-U., and Hamilton, D. P. (2002a). A tenuous dust ring of Jupiter formed by escaping ejecta from the Galilean satellites. *J. Geophys. Res.*, 107:E1, 10.1029/2000JE001434.
- Krivov, A. V., Sremčević, M., Spahn, F., Dikarev, V. V., and Kholshchevnikov, K. V. (2003). Impact-generated dust clouds around planetary satellites: Spherically-symmetric case. *Planetary and Space Science*, 51:251–269.
- Krivov, A. V., Wardinski, I., Spahn, F., Krüger, H., and Grün, E. (2002b). Dust on the outskirts of the Jovian system. *Icarus*, 157:436–455.

- Krüger, H. and Grün, E. (2002). Dust en-route to Jupiter and the Galilean satellites. In Green, S. F., Williams, I., McDonnell, T., and McBride, N., editors, *Cospar Colloquia series Vol. 15*, Dust in the solar system and in other planetary systems, pages 144–159. Pergamon Press.
- Krüger, H., Grün, E., Graps, A. L., Bindschadler, D. L., Dermott, S. F., Fechtig, H., Gustafson, B. A., Hamilton, D. P., Hanner, M. S., Horányi, M., Kissel, J., Lindblad, B., Linkert, D., Linkert, G., Mann, I., McDonnell, J. A. M., Morfill, G. E., Polanskey, C., Schwehm, G. H., Srama, R., and Zook, H. A. (2001). One year of Galileo dust data: 1996. *Planetary and Space Science*, 49:1285–1301.
- Krüger, H., Grün, E., Graps, A. L., and Lammers, S. (1999a). Observations of electromagnetically coupled dust in the Jovian magnetosphere. In J. Büchner, I. Axford, E. M. and Vasyliunas, V., editors, *Proceedings of the VII. International Conference on Plasma Astrophysics and Space Physics, held in Lindau in May 1998*, volume 264, pages 247–256. Kluwer Academic Publishers.
- Krüger, H., Grün, E., Hamilton, D. P., Baguhl, M., Dermott, S. F., Fechtig, H., Gustafson, B. A., Hanner, M. S., Horányi, M., Kissel, J., Lindblad, B. A., Linkert, D., Linkert, G., Mann, I., McDonnell, J. A. M., Morfill, G. E., Polanskey, C., Riemann, R., Schwehm, G. H., Srama, R., and Zook, H. A. (1999b). Three years of Galileo dust data: II. 1993 to 1995. *Planetary and Space Science*, 47:85–106.
- Krüger, H., Grün, E., Heck, A., and Lammers, S. (1999c). Analysis of the sensor characteristics of the Galileo dust detector with collimated Jovian dust stream particles. *Planetary and Space Science*, 47:1015–1028.
- Krüger, H., Horányi, M., and Grün, E. (2003a). Jovian dust streams: Probes of the Io plasma torus. *Geophysical Research Letters*, 30(2):1058, doi:10.1029/2002GL015920.
- Krüger, H., Horányi, M., Krivov, A. V., and Graps, A. L. (2003b). Jovian Dust: Streams, Clouds and Rings. In Bagenal, F., McKinnon, B., and Dowling, T., editors, *Jupiter: Planet, Satellites & Magnetosphere*. Cambridge University Press. accepted.
- Krüger, H., Krivov, A. V., and Grün, E. (2000). A dust cloud of Ganymede maintained by hypervelocity impacts of interplanetary micrometeoroids. *Planetary and Space Science*, 48:1457–1471.
- Krüger, H., Krivov, A. V., Hamilton, D. P., and Grün, E. (1999d). Detection of an impact-generated dust cloud around Ganymede. *Nature*, 399:558–560.
- Landgraf, M., Baggeley, W. J., Grün, E., Krüger, H., and Linkert, G. (2000). Aspects of the Mass Distribution of Interstellar Dust Grains in the Solar System from in situ Measurements. *J. Geophys. Res.*, 105, no. A5:10,343–10352.
- Morfill, G. E., Grün, E., and Johnson, T. V. (1980). Dust in Jupiter’s magnetosphere - Origin of the Ring. *Planetary and Space Science*, 28:1101–1110.

- Ockert-Bell, M. E., Burns, J. A., Daubar, I. J., Thomas, P. C., Veverka, J., Belton, M. J. S., and Klaasen, K. P. (1999). The structure of Jupiter's ring system as revealed by the Galileo imaging experiment. *Icarus*, 138:188–213.
- Soter, S. (1971). The dust belts of Mars. Technical report, Center for Radiophysics and Space Research Report No. 462.
- Srama, R., Ahrens, T. J., Altobelli, N., Auer, S., Bradley, J. G., Burton, M., Dikarev, V. V., Fechtig, H., Görlich, M., Grande, M., Graps, A. L., Grün, E., Havnes, O., Helfert, S., Horányi, M., Igenbergs, E., Jeßberger, E. K., Johnson, T. V., Kempf, S., Krivov, A. V., Krüger, H., Moragas-Klostermeyer, G., Lamy, P., Landgraf, M., Linkert, D., Linkert, G., Lura, F., McDonnell, J. A. M., Möhlmann, D., Morfill, G. E., Müller, M., Schäfer, G., Schlotzhauer, G. H., Schwehm, G. H., Spahn, F., Stübig, M., Svestka, J., Tschernjawski, V., Tuzzolino, A. J., Wäsch, R., and Zook, H. A. (2002). The Cassini Cosmic Dust Analyzer. *Space Science Reviews*. submitted.
- Sremčević, M., Krivov, A. V., and Spahn, F. (2003). Impact-generated dust clouds around planetary satellites: Asymmetry effects. *Planetary and Space Science*. in press.
- Thiessenhusen, K.-U., Krivov, A. V., Krüger, H., and Grün, E. (2002). A dust cloud around Pluto and Charon. *Planetary and Space Science*, 50:79–87.
- Thiessenhusen, K.-U., Krüger, H., Spahn, F., and Grün, E. (2000). Dust grains around Jupiter – The observations of the Galileo Dust Detector. *Icarus*, 144:89–98.
- Zook, H. A., Grün, E., Baguhl, M., Hamilton, D. P., Linkert, G., Linkert, D., Liou, J.-C., Forsyth, R., and Phillips, J. L. (1996). Solar wind magnetic field bending of Jovian dust trajectories. *Science*, 274:1501–1503.

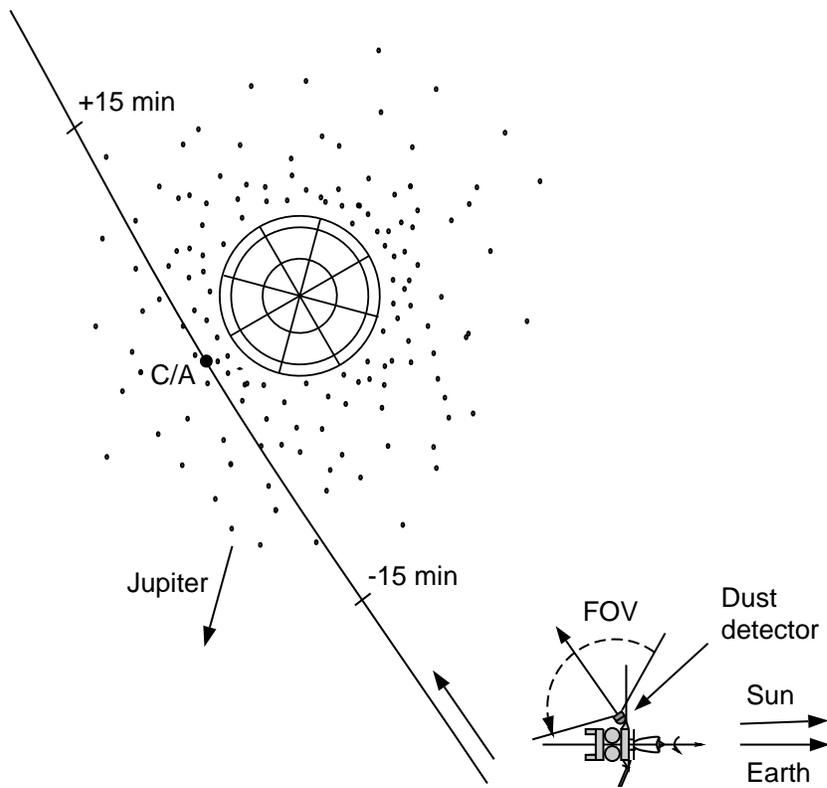


Figure 1: Galileo's trajectory and geometry of dust detection during the E4 Europa flyby. The Galileo spacecraft is sketched in an orientation it was in during the flyby (see text for details). The directions to Jupiter, Earth and Sun are shown. C/A indicates closest approach to Europa, FOV the field of view of the dust instrument. The orientation of the dust instrument shown corresponds to a rotation angle  $\Theta = 270^\circ$ . At  $90^\circ$  rotation angle it points in the opposite direction.

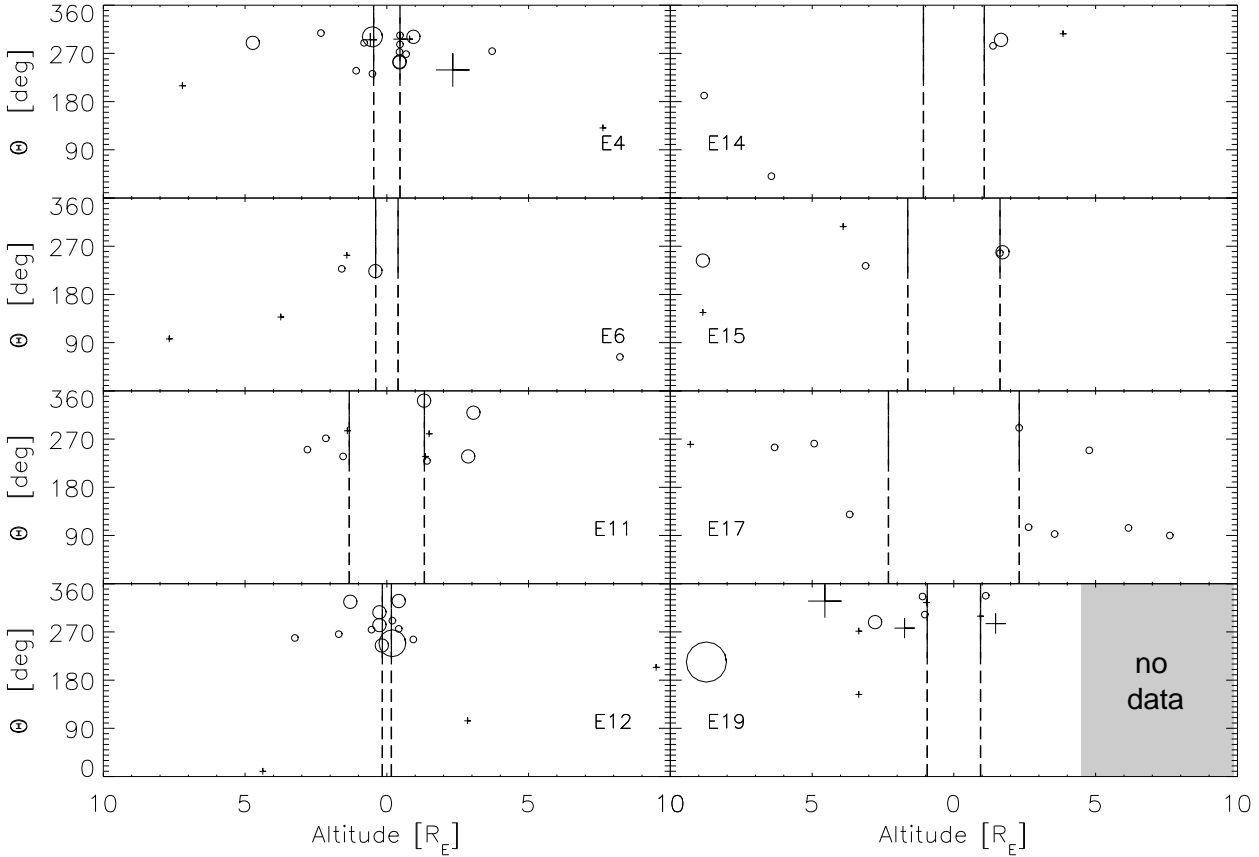


Figure 2: Sensor direction (rotation angle,  $\Theta$ ) versus altitude of the Galileo spacecraft above the surface of Europa at the time of dust impact. Data are shown for all eight Europa encounters during which data were successfully collected (E4, E6, E11, E12, E14, E15, E17, E19). The radius of Europa,  $R_E$  is given in Table I. The altitude range shown corresponds to a time interval of 2 h. Each symbol indicates a dust particle impact, and the size of the symbol indicates the impact charge created by the particle ( $10^{-14} \text{ C} \leq Q_I \leq 10^{-9} \text{ C}$ ). Circles show particles with impact speeds below  $10 \text{ km s}^{-1}$  and crosses show particles with higher speeds. Galileo did not traverse the region between the vertical dashed lines. In E19 no data were collected later than 19 min after closest approach (corresponding to  $4.5 R_E$  altitude) because of a spacecraft anomaly. Noise events have been removed (Krüger et al., 2001, their Table 4).

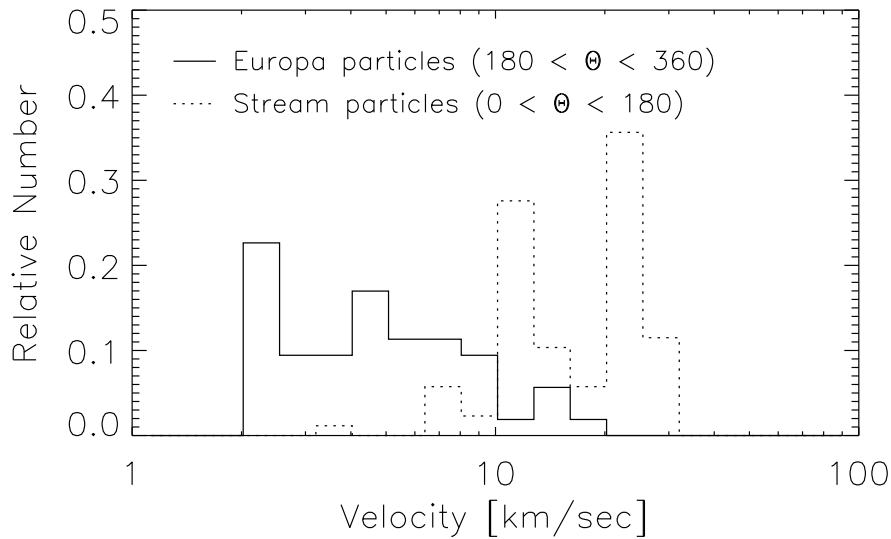


Figure 3: Impact speeds derived from the instrument calibration for dust particles detected below  $8 R_E$  altitude at eight Europa encounters. The solid line shows the distribution for Europa particles ( $180^\circ \leq \Theta \leq 360^\circ$ ) and the dotted line that for stream particles ( $0^\circ \leq \Theta \leq 180^\circ$ ). The mean impact speed is  $5.5 \pm 3.5 \text{ km s}^{-1}$ . Only particles with a velocity error factor  $VEF < 6$  (Grün et al., 1995) have been considered (53 Europa particles).

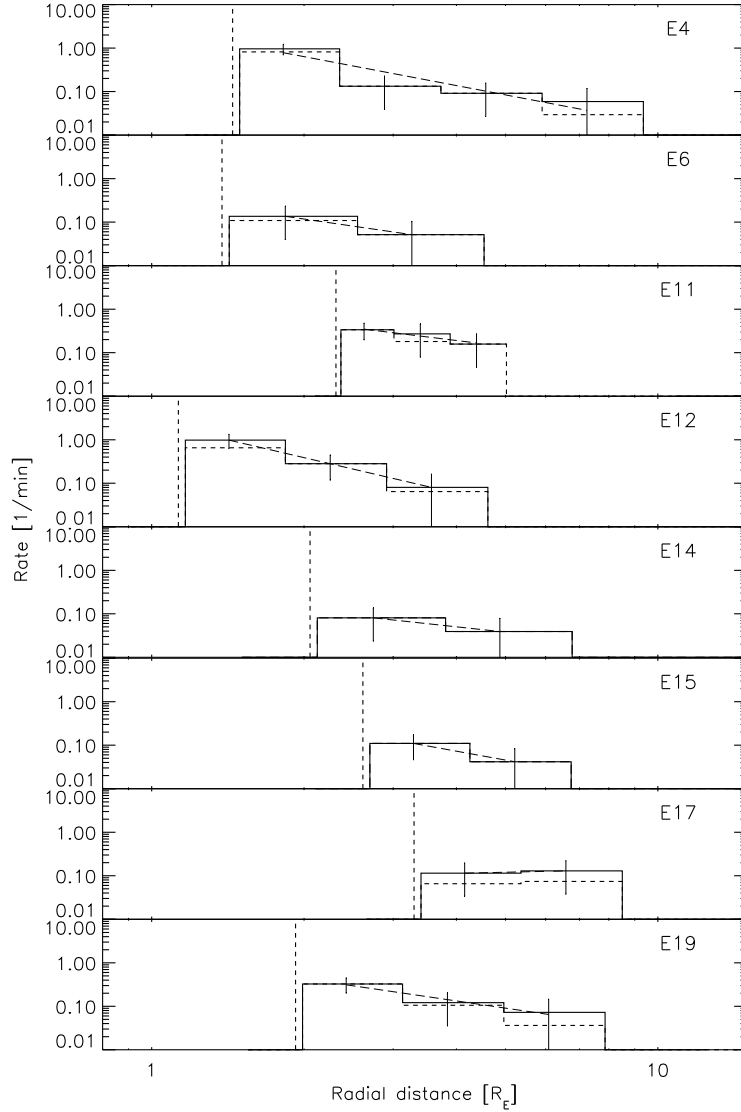


Figure 4: Impact rates of dust particles detected during eight Europa encounters. The dotted histogram bins show the impact rates derived from the number of particles in each bin for which their complete information has been transmitted to Earth. The solid histograms show the same rates, but corrected for incomplete data transmission. In cases where only a solid line is visible, no correction was necessary because the complete information of all particle impacts is available in that bin. The vertical dotted lines indicate the minimum altitude reached by Galileo at closest approach. Error bars denote the  $\sqrt{N}$  statistical uncertainty, with  $N$  being the number of particles for which the complete information has been transmitted. Dashed lines are power law fits to the corrected impact rate (Table II). In E17 data were collected with a low rate of one instrument readout every 7 min which leads to a larger uncertainty in the impact time. Therefore, the impact time of the dust particles was shifted by  $-3.5$  min to compensate for the reduced time resolution. At E19, no data were collected beyond  $4.5 R_E$  after Europa closest approach and the impact rate shown was multiplied by two outside this region to empirically correct for the missing data.

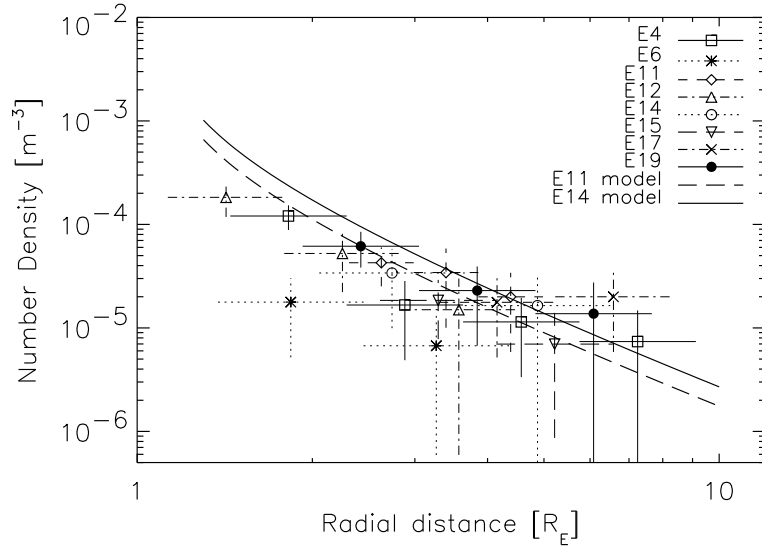


Figure 5: The number density of dust as a function of distance from the center of Europa, derived from the data (symbols with error bars) and predicted by the model (Krivov et al., 2003, lines). Horizontal bars for the data symbols indicate distance bins which were used in processing the data (see text for details), whereas vertical ones reflect  $\sqrt{N}$  errors due to a limited number of impacts. Since dust impacts are measured above a certain speed-dependent detection threshold of the instrument, different flyby speeds imply different minimum mass of the detected grains and therefore should give different dust number densities. This has been taken into account in the model. Two model curves are shown: for the slowest (E11) and the fastest flyby (E14).

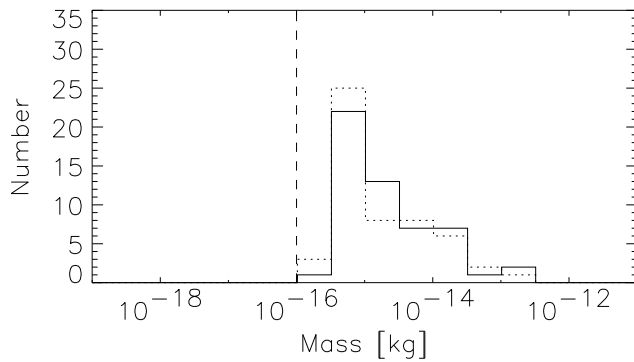
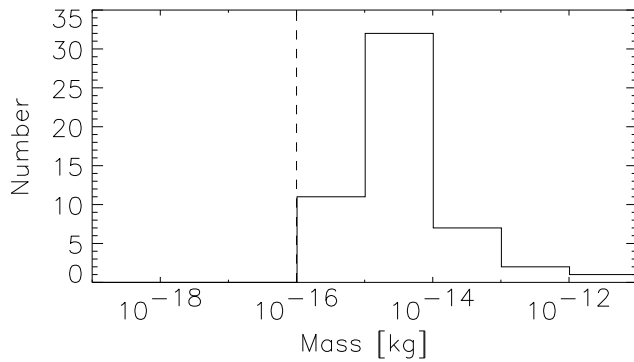


Figure 6: Mass distribution of the particles detected during eight Europa flybys. The upper panel shows the distribution obtained by using the measured impact speeds derived from the instrument calibration. In the lower panel the speed of Galileo relative to Europa has been assumed as the impact velocity in order to calculate the particle mass. The dotted histogram is without aging correction, the data for the solid histogram has been corrected for aging of the dust detector electronics. The vertical dashed lines indicate the detection threshold for particles which approach the detector with the velocity of Galileo relative to Europa (about  $6 \text{ km s}^{-1}$ ). Only the 53 particles with a velocity error factor  $\text{VEF} < 6$  (Grün et al., 1995) have been considered.

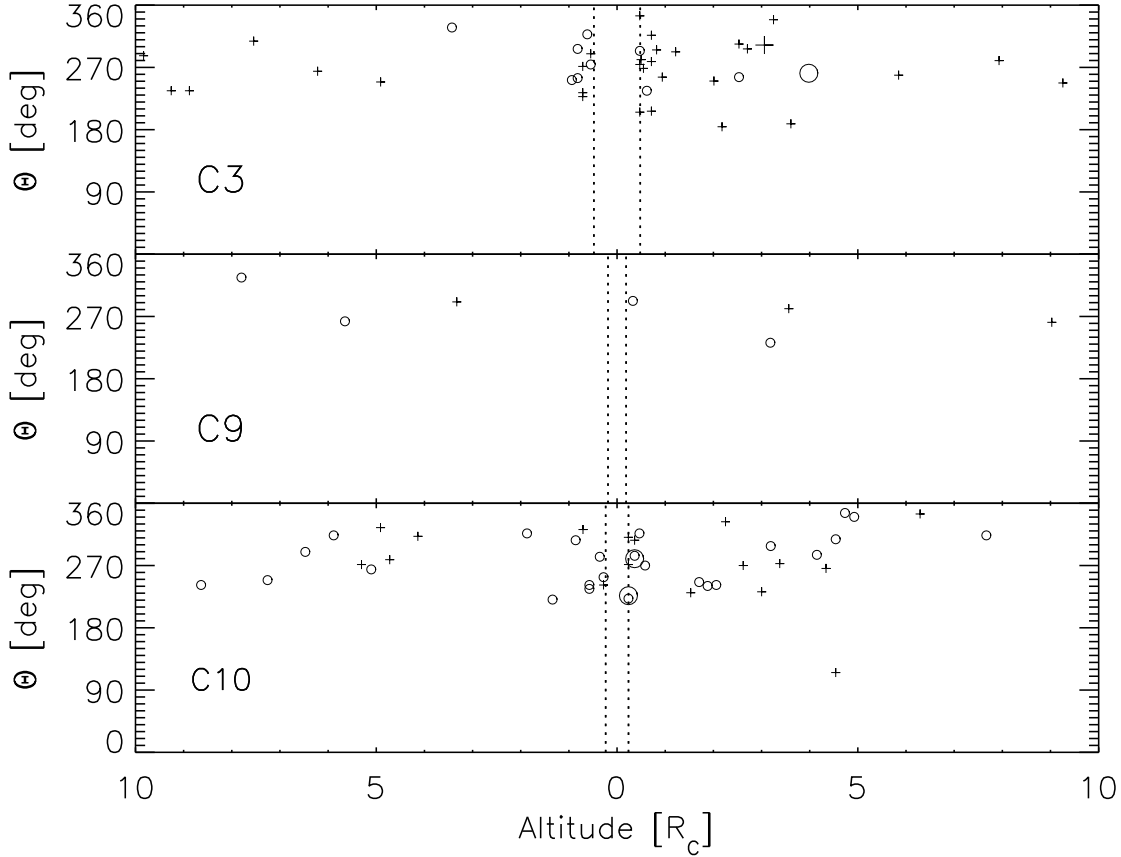


Figure 7: Sensor direction (rotation angle,  $\Theta$ ) versus altitude of the Galileo spacecraft above the surface of Callisto at the time of dust impact. Data are shown for all three Callisto encounters at which the spacecraft orientation allowed the detection of cloud particles (C3, C9, C10). The radius of Callisto,  $R_C$ , is given in Table I. The altitude range shown corresponds to a time interval of 2 h. Each symbol indicates a dust particle impact, and the size of the symbol indicates the impact charge created by the particle ( $10^{-14} \text{ C} \leq Q_I \leq 10^{-13} \text{ C}$ ). Circles show particles with impact speeds below  $10 \text{ km s}^{-1}$  and crosses show particles with higher speeds. Galileo did not traverse the region between the vertical dashed lines.

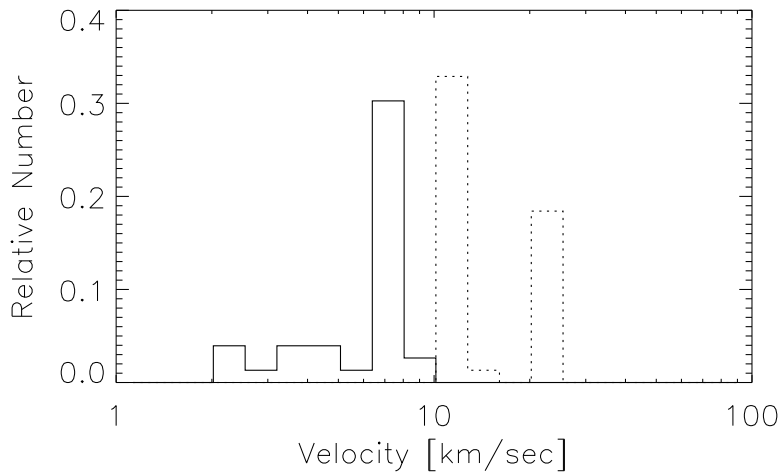


Figure 8: Impact speeds derived from the instrument calibration for dust particles detected at all three Callisto encounters below  $6 R_C$  altitude with  $180^\circ \leq \Theta \leq 360^\circ$  and calibrated impact velocities below  $10 \text{ km s}^{-1}$  (solid line) and above  $10 \text{ km s}^{-1}$  (dotted line). Only particles with a velocity error factor  $VEF < 6$  (Grün et al., 1995) have been considered (35 particles with  $10 \text{ km s}^{-1}$ ).

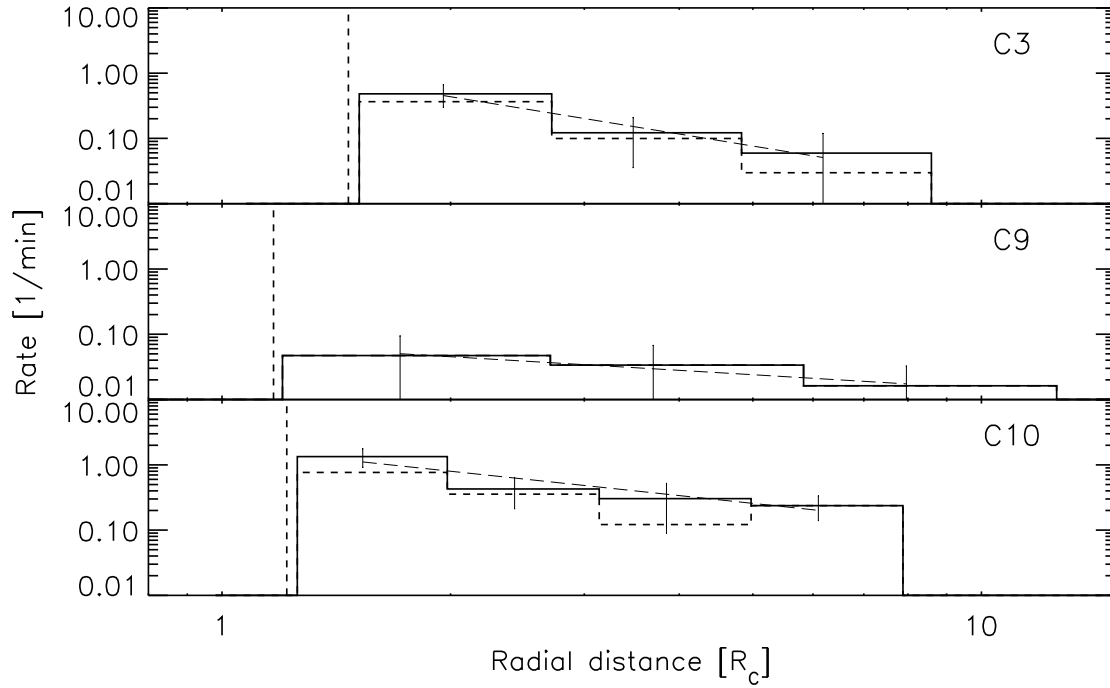


Figure 9: Impact rates of dust particles detected during three Callisto encounters. Same notation as in Fig. 4. Only particles with impact speed  $< 10 \text{ km s}^{-1}$  have been considered and no noise removal has been applied.

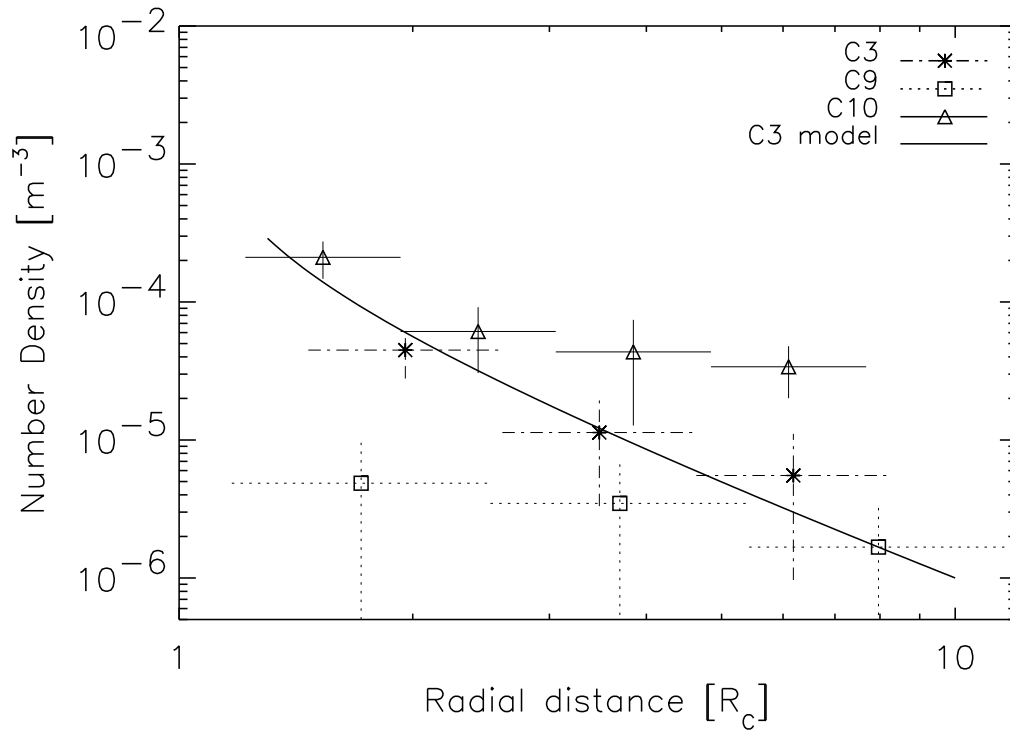


Figure 10: Same as Fig. 5 but for Callisto. The theoretical profiles for C9 and C10 are very close to the one which is plotted for C3.

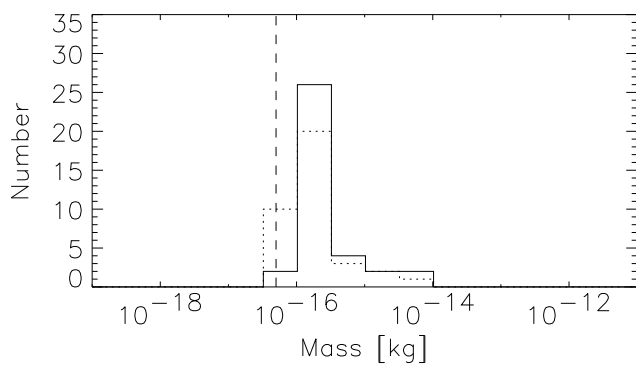
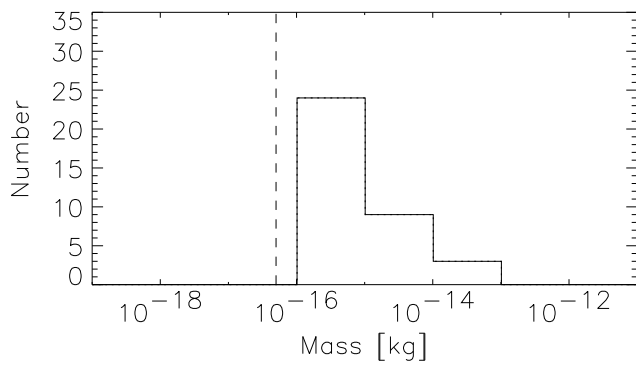


Figure 11: Same as Fig. 6 but for three Callisto flybys. The detection threshold is shown for  $8 \text{ km s}^{-1}$ . Only the 35 particles with a velocity error factor  $\text{VEF} < 6$  (Grün et al., 1995) have been considered. The dotted histogram is without aging correction, the data for the solid histogram has been corrected for aging of the dust detector electronics.

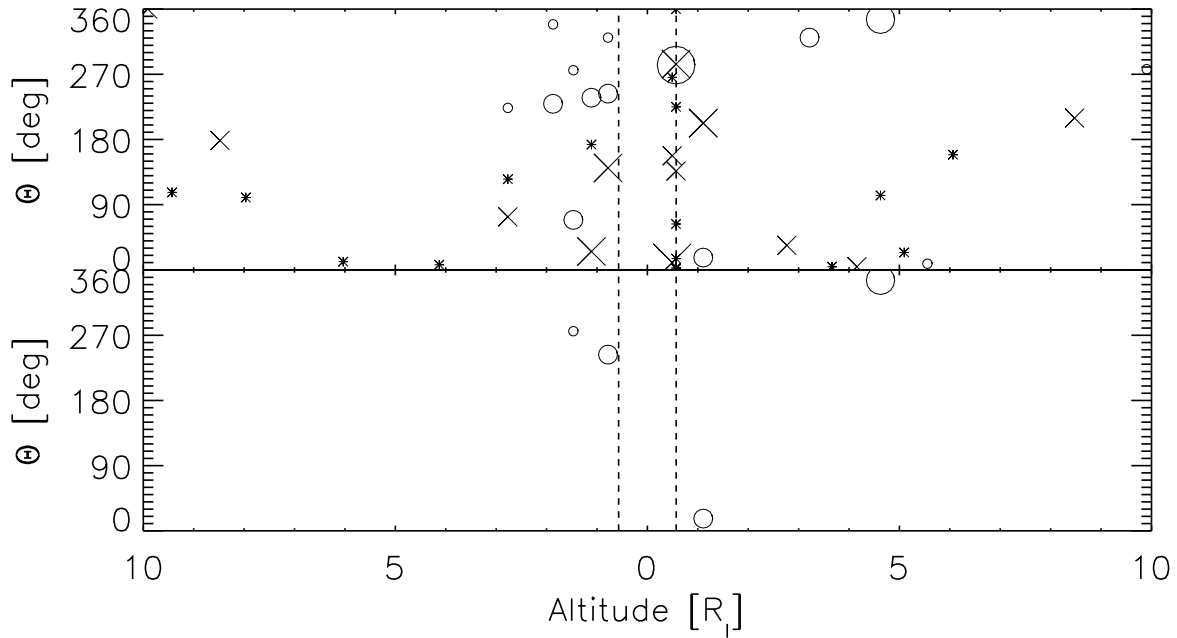


Figure 12: Sensor direction (rotation angle,  $\Theta$ ) versus altitude of the Galileo spacecraft above the surface of Io at the time of dust impact for the I0 flyby. The radius of Io,  $R_I$  is given in Table I. The altitude range shown corresponds to a time interval of about 45 min. Each symbol indicates an impact event (dust or noise), and the size of the symbol indicates the generated charge ( $2 \times 10^{-14} \text{ C} \leq Q_I \leq 10^{-8} \text{ C}$ ). Circles show class 2 and class 3, asterisks show class 1 in the lowest amplitude range, crosses denote class 1, amplitude range 2 and higher. Top panel: all data in classes 1 to 3, bottom panel: class 3 and noise-removed class 2 data.

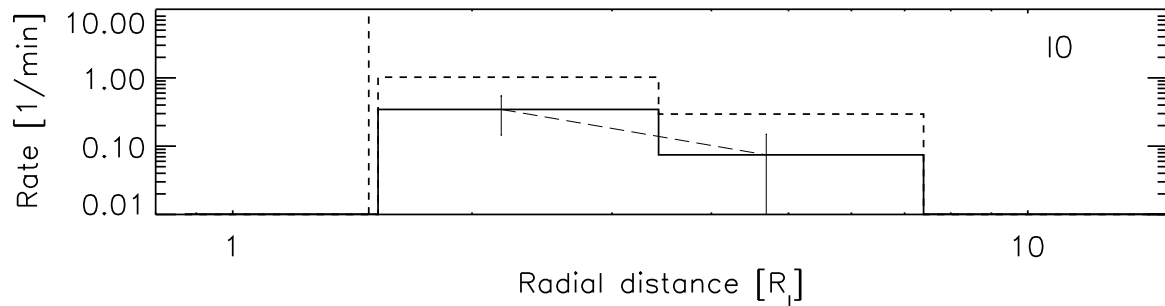


Figure 13: Impact rates of dust particles detected during Galileo's I0 encounter of Io. Same notation as in Fig. 4. Solid histogram: class 3 and noise-removed class 2 data (derived from only four dust impacts), dashed histogram: class 3 and all class 2 data (without noise removal).

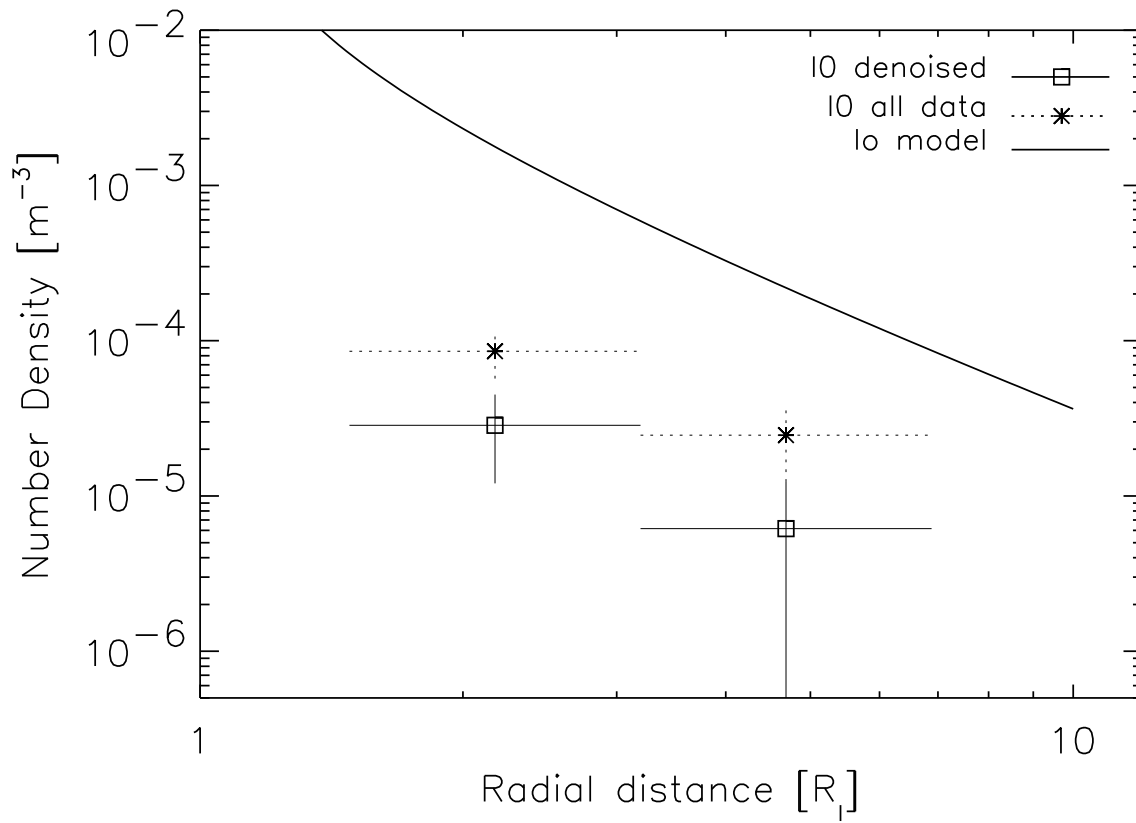


Figure 14: Same as Fig. 5 but for Io. Class 3 and noise-removed class 2 data are shown with solid lines. All class 3 and class 2 data taken together are shown with dotted lines.

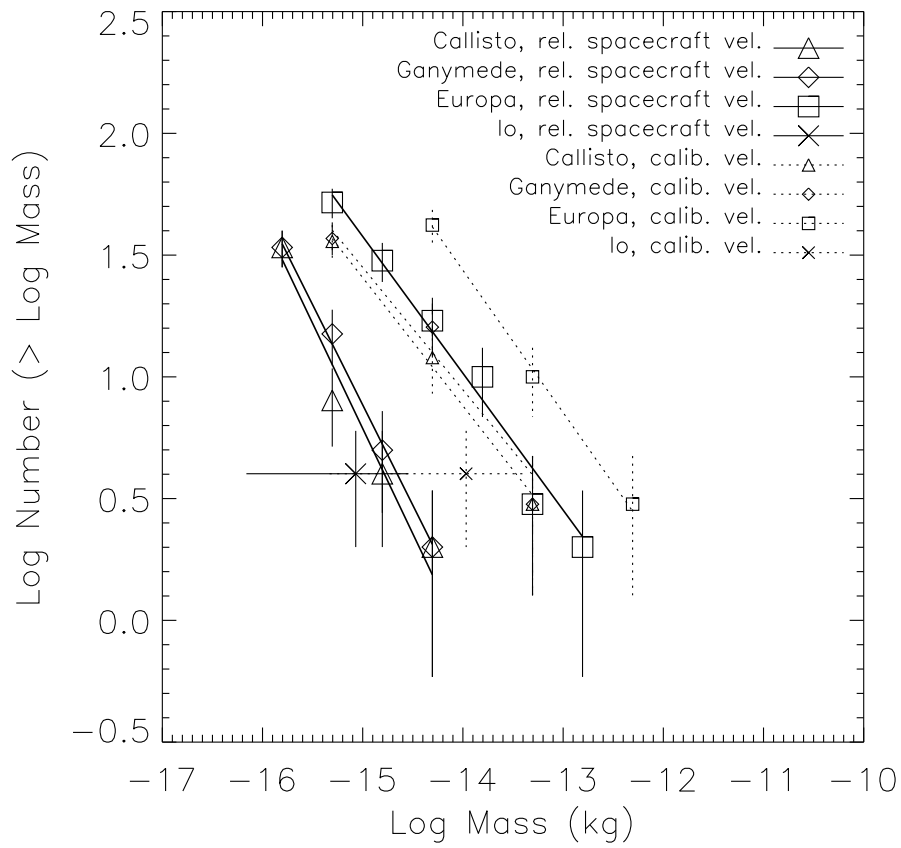


Figure 15: Cumulative mass distributions from Fig. 6 and 11 for Europa and Callisto, respectively, and from Krüger et al. (2000) for Ganymede. For Io only one data point is shown because of the scarcity of the data. Straight lines are linear fits to the data. Vertical bars indicate the  $\sqrt{N}$  statistical uncertainty.

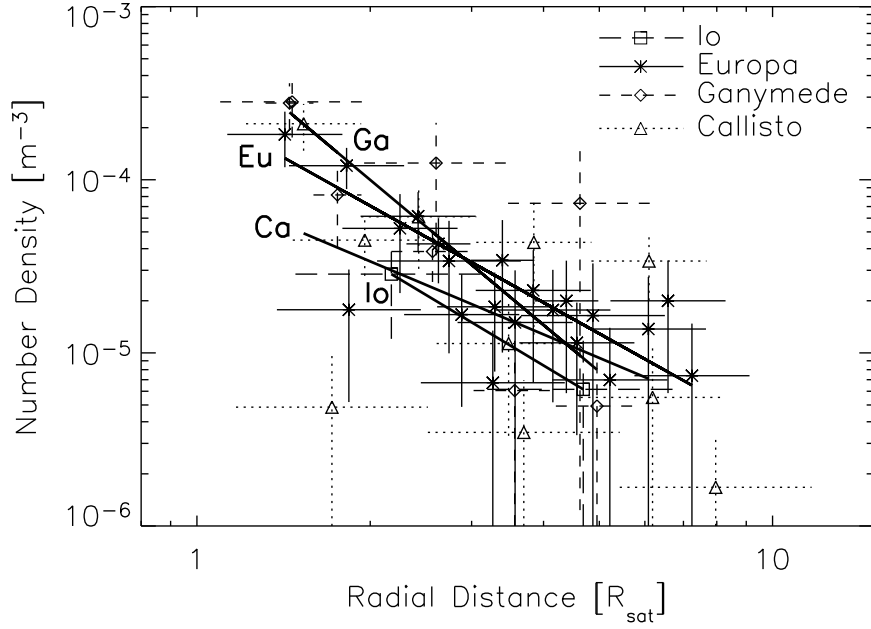


Figure 16: Number density of dust as a function of radial distance from the center of Ganymede (data from 4 flybys), Europa (8 flybys), Callisto (3 flybys) and Io (1 flyby). The altitude is shown in units of the satellite radius (Tab I). Vertical error bars reflect statistical uncertainty due to the small number of impacts. The straight lines are mean measured curves for each moon (Table IV, col. 8)

Table I: Physical properties of Jupiter and the Galilean satellites used in this paper. The Hill radius is defined as  $r_{\text{Hill}} = r(\frac{m}{3(M+m)})^{1/3}$  with  $M, m$  being the masses of Jupiter and the moon, separated by distance  $r$ .

Object	Jovicentric distance ( $R_J$ )	Radius $r_{\text{obj}}$ (km)	Symbol	Hill radius $r_{\text{Hill}}$ ( $R_{\text{obj}}$ )	Escape speed $v_{\text{esc}}$ ( $\text{km s}^{-1}$ )
Jupiter	–	71,492	$R_J$	–	–
Io	5.9	1,818	$R_I$	5.8	2.56
Europa	9.4	1,560	$R_E$	8.7	2.03
Ganymede	15.0	2,634	$R_G$	12.0	2.74
Callisto	26.3	2,409	$R_C$	20.9	2.44

Table II: Galileo flyby characteristics and parameters for the dust particles detected during Galileo’s flybys at Europa, Callisto and Io (for Europa, particles within  $8 R_E$  altitude have been included, and for Callisto and Io within  $6 R_C$  and  $6 R_I$ , respectively): Flyby number (col. 1), time of flyby (col. 2), altitude at closest approach to satellite (col. 3), velocity of Galileo relative to satellite (col. 4), average measured particle velocity (velocity error factor  $VEF < 6$ , Grün et al. (1995); col. 5), spin-averaged sensor area (maximum value  $235 \text{ cm}^2$ ; col. 6), number of class 2 and class 3 satellite particles for which their complete data set has been transmitted to Earth ( $180^\circ < \Theta < 360^\circ$ ; col. 7), number of all events (dust plus noise) detected with  $180^\circ < \Theta < 360^\circ$  (both within  $8 R_E$ , col. 8), completeness of data set due to incomplete data transmission of Galileo (col. 9) and slope of power law fit to the radial variation of the impact rate (Fig. 4, 9, 13; col. 10). The slopes are weighted with the square root of the number of particles, and the uncertainty takes into account the error bar of each data point. Values given in parentheses have been derived from only four or fewer particles.

Flyby	Date	Altitude	Spacecraft velocity	Average particle velocity	Sensor area	Particles with full data sets	All events with full data sets	Completeness of data set	Slope of impact rate
(1)	(Year-Day)	(km)	( $\text{km s}^{-1}$ )	( $\text{km s}^{-1}$ )	( $\text{cm}^2$ )	(7)	(8)	(%)	(10)
Europa									
E4	96-354.287	698	5.7	$6.8 \pm 4.0$	233	18	23	86	$-2.21 \pm 0.36$
E6	97-051.713	586	5.7	$5.9 \pm 4.0$	224	3	7	88	$(-1.69 \pm 0.58)$
E11	97-310.855	2,043	5.6	$5.5 \pm 2.2$	235	10	11	90	$-1.43 \pm 2.25$
E12	97-350.502	201	6.3	$4.5 \pm 1.7$	142	12	13	61	$-2.72 \pm 0.91$
E14	98-088.556	1,644	6.5	$3.4 \pm 1.3$	61	3	4	100	$(-1.26 \pm 0.44)$
E15	98-151.884	2,515	6.4	$5.5 \pm 1.5$	155	4	6	100	$(-2.11 \pm 0.59)$
E17	98-269.163	3,582	6.0	$2.8 \pm 0.8$	180	4	4	54	$(+0.27 \pm 1.56)$
E19	99-032.097	1,439	5.8	$5.7 \pm 4.7$	152	$10^\dagger$	$13^\dagger$	$100^\dagger$	$-1.70 \pm 0.62$
Callisto									
C3	96-309.566	1,118	8.0	$6.3 \pm 1.7$	224	10	35	80	$-1.90 \pm 0.45$
C9	97-176.575	415	8.2	$7.6 \pm 0.2$	197	3	5	100	$(-0.69 \pm 0.10)$
C10	97-260.013	538	8.2	$6.3 \pm 2.3$	142	22	37	64	$-1.31 \pm 1.06$
Io									
I0	95-341.740	892	15.0	$10.3 \pm 8.4$	133	4	13	87	$(-2.00 \pm 1.88)$

†: Data transmission ceased 1 Feb 99, 02:38:46h, *i.e.* 19 min after closest approach, at 6,767 km altitude. All data sets of particles detected earlier during the E19 encounter were transmitted.

Table III: Model parameters for different satellites: speed of impactors, geometric albedo, assumed silicate content, energy partitioning parameter, characteristic yield, parameters of the ejecta speed distribution (see Krivov et al. 2002b for description of the parameters).

Satellite	$v_{\text{imp}}$ ( $\text{km s}^{-1}$ )	$A$	$G_{\text{sil}}$	$K_e/K_i$ (%)	$Y$	$u_0$ ( $\text{m s}^{-1}$ )	$\gamma$
Io	26	0.61	0	30	$2.8 \times 10^4$	28	2.0
Europa	21	0.64	0	30	$1.6 \times 10^4$	30	2.0
Callisto	15	0.20	70	20	$7.1 \times 10^2$	51	1.4

Table IV: Derived properties of the impact-generated dust clouds (data for Ganymede taken from Krüger et al. (2000)): mean flyby speed of Galileo at the satellite (col. 2), number of detected cloud particles for which the complete data set has been transmitted (col. 3), mean measured impact speed of these particles ( $VEF < 6$ ; col. 4), mean particle mass (col. 5), corresponding particle radius assuming spherical particles with density  $1 \text{ g cm}^{-3}$  (col. 6), slope of the power law fit to the cumulative mass distribution (col. 7) and average slope of radial number density distribution (col. 8; averages of slopes from individual flybys). The speed of Galileo relative to the satellite has been assumed for the values in col. 5 to 7. For the uncertainties in the number density slopes (col. 8) the uncertainties of the slopes from each individual flyby have been taken into account.

Object	Average flyby speed ( $\text{km s}^{-2}$ )	Number of detections	Average particle speed ( $\text{km s}^{-2}$ )	Average particle mass (kg)	Average particle radius ( $\mu\text{m}$ )	Slope $\alpha$ of mass distrib.	Slope of radial number density distrib.
(1)	(2)	(3)	(4)	(5)	(6)	(7)	(8)
Io	15.0	4	$10.3 \pm 8.4$	$8.5 \times 10^{-16}$	$\approx 0.6$	–	(–2.00)
Europa	6.0	64	$5.5 \pm 3.5$	$1.3 \times 10^{-14}$	$\approx 1.0$	$0.58 \pm 0.04$	$-2.02 \pm 0.63$
Ganymede	8.2	38	$7.2 \pm 4.9$	$9.5 \times 10^{-16}$	$\approx 0.6$	$0.82 \pm 0.04$	$-2.82 \pm 2.60$
Callisto	7.2	35	$6.4 \pm 2.1$	$5.2 \times 10^{-16}$	$\approx 0.5$	$0.86 \pm 0.14$	$-1.60 \pm 0.39$

Table V: Mass budgets of the dust clouds (model estimates, see Krivov et al. 2002b for description of the model).

Satellite	Io	Europa	Ganymede	Callisto
Mass flux of impactors [ $\text{g m}^{-2} \text{ s}^{-1}$ ]	$1 \times 10^{-11}$	$7 \times 10^{-12}$	$4 \times 10^{-12}$	$3 \times 10^{-12}$
Mass inflow of impactors [ $\text{g s}^{-1}$ ]	130	50	100	50
Yield	$3 \times 10^4$	$2 \times 10^4$	$4 \times 10^3$	$7 \times 10^2$
Mass production rate of ejecta [ $\text{g s}^{-1}$ ]	$4 \times 10^6$	$9 \times 10^5$	$4 \times 10^5$	$3 \times 10^4$
Mean lifetime of ejecta [ $\text{s}$ ] <sup>a)</sup>	50	70	120	250
Steady-state mass of the cloud [tons]	200	60	40	9
Fraction of escaping ejecta	$1 \times 10^{-4}$	$2 \times 10^{-4}$	$8 \times 10^{-4}$	$4 \times 10^{-3}$
Ejection rate into circumjovian space [ $\text{g s}^{-1}$ ]	400	200	300	100

<sup>a)</sup> Residence time within the Hill sphere before recollision or escape